Cellular/Molecular

SIPA1L1/SPAR1 Interacts with the Neurabin Family of Proteins and is Involved in GPCR Signaling

Ken Matsuura,[1,8] Shizuka Kobayashi,[2] Kohtarou Konno,[3] Miwako Yamasaki,[3] Takahiro Horiuchi,[4] Takao Senda,[5] Tomoatsu Hayashi,[1] Kiyotoshi Satoh,[1] Fumiko Arima-Yoshida,[2] Kei Iwasaki,[1] Lumi Negishi,[1] Naomi Yasui-Shimizu,[1] Kazuyoshi Kohu,[1] Shigenori Kawahara,[4,6] Yutaka Kirino,[4,7] Tsutomu Nakamura,[1] Masahiko Watanabe,[3] Tadashi Yamamoto,[8] Toshiya Manabe,[2] and Tetsu Akiyama[1]

[1]Laboratory of Molecular and Genetic Information, Institute for Quantitative Biosciences, The University of Tokyo, Bunkyo-ku, Tokyo 113-0032, Japan, [2]Division of Neuronal Network, Department of Basic Medical Sciences, Institute of Medical Science, The University of Tokyo, Minato-ku, Tokyo 108-8639, Japan, [3]Department of Anatomy, Hokkaido University Graduate School of Medicine, Sapporo 060-8638, Japan, [4]Laboratory of Neurobiophysics, School of Pharmaceutical Sciences, The University of Tokyo, Tokyo 113-0033, Japan, [5]Department of Anatomy, Graduate School of Medicine, Gifu University, Gifu 501-1194, Japan, [6]Graduate School of Science and Engineering, University of Toyama, Toyama 930-8555, Japan, [7]Kagawa School of Pharmaceutical Sciences, Tokushima Bunri University, Sanuki, Kagawa 769-2101, Japan, and [8]Cell Signal Unit, Okinawa Institute of Science and Technology, Onna-son 904-0495, Japan

Signal-induced proliferation-associated 1 (SIPA1)-like 1 (SIPA1L1; also known as SPAR1) has been proposed to regulate synaptic functions that are important in maintaining normal neuronal activities, such as regulating spine growth and synaptic scaling, as a component of the PSD-95/NMDA-R-complex. However, its physiological role remains poorly understood. Here, we performed expression analyses using super-resolution microscopy (SRM) in mouse brain and demonstrated that SIPA1L1 is mainly localized to general submembranous regions in neurons, but surprisingly, not to PSD. Our screening for physiological interactors of SIPA1L1 in mouse brain identified spinophilin and neurabin-1, regulators of G-protein-coupled receptor (GPCR) signaling, but rejected PSD-95/NMDA-R-complex components. Furthermore, *Sipa1l1*$^{-/-}$ mice showed normal spine size distribution and NMDA-R-dependent synaptic plasticity. Nevertheless, *Sipa1l1*$^{-/-}$ mice showed aberrant responses to α_2-adrenergic receptor (a spinophilin target) or adenosine A1 receptor (a neurabin-1 target) agonist stimulation, and striking behavioral anomalies, such as hyperactivity, enhanced anxiety, learning impairments, social interaction deficits, and enhanced epileptic seizure susceptibility. Male mice were used for all experiments. Our findings revealed unexpected properties of SIPA1L1, suggesting a possible association of SIPA1L1 deficiency with neuropsychiatric disorders related to dysregulated GPCR signaling, such as epilepsy, attention deficit hyperactivity disorder (ADHD), autism, or fragile X syndrome (FXS).

Key words: GPCR; neurabin; PSD; SIPA1L1; SPAR; spinophilin

Significance Statement

Signal-induced proliferation-associated 1 (SIPA1)-like 1 (SIPA1L1) is thought to regulate essential synaptic functions as a component of the PSD-95/NMDA-R-complex. In our screening for physiological SIPA1L1-interactors, we identified G-protein-coupled receptor (GPCR)-signaling regulators. Moreover, SIPA1L1 knock-out (KO) mice showed striking behavioral anomalies, which may be relevant to GPCR signaling. Our findings revealed an unexpected role of SIPA1L1, which may open new avenues for research on neuropsychiatric disorders that involve dysregulated GPCR signaling. Another important aspect of this paper is that we showed effective methods for checking PSD association and identifying native protein interactors that are difficult to solubilize. These results may serve as a caution for future claims about interacting proteins and PSD proteins, which could eventually save time and resources for researchers and avoid confusion in the field.

Received Mar. 18, 2021; revised Dec. 28, 2021; accepted Jan. 10, 2022.

Author contributions: K.M., S.Ko., K.Kon., M.Y., T.Ho., T.S., T.Ha., K.S., K.I., L.N., K.Koh., S.Ka., Y.K., T.N., M.W., T.Y., T.M., and T.A. designed research; K.M., S.Ko., K.Kon., M.Y., T.Ho., T.S., T.Ha., K.S., F.A.-Y., K.I., L.N., and N.Y.-S. performed research; T.Y. contributed unpublished reagents/analytic tools; K.M., S.Ko., K.Kon., and T.Ho. analyzed data; K.M. wrote the first draft of the paper; K.M., T.N., T.M., and T.A. edited the paper; K.M. and T.A. wrote the paper.

This work was supported by JSPS (Japan Society for the Promotion of Science) Grants-in-Aid for Scientific Research KAKENHI Grant Numbers JP24790311 and JP26460385. We thank Yutaka Yoshida at Okinawa Institute of Science and Technology (OIST) for critical reading of the manuscript and useful suggestions, Hiroshi Toriyama, Toshihiro Maruyama, and Miyuki Koumura at The University of Tokyo Institute for Quantitative Biosciences Olympus Bioimaging Center (TOBIC) for technical assistance with Olympus microscopes; the OIST Imaging Section and Paolo Barzaghi for their support with SD-OSR (Spinning Disk - Olympus Super Resolution) microscope; and Masaki Sagara and Yoshihiro Kawasaki for providing plasmid constructs of spinophilin mutants.

The authors declare no competing financial interests.

Correspondence should be addressed to Ken Matsuura at ken.matsuura@oist.jp or Tetsu Akiyama at akiyama@iqb.u-tokyo.ac.jp.

https://doi.org/10.1523/JNEUROSCI.0569-21.2022

Introduction

Signal-induced proliferation-associated 1 (SIPA1)-like 1 (SIPA1L1) was identified as a PSD protein and a component of the PSD-95/NMDA-R complex in neurons (Pak et al., 2001). SIPA1L1 is comprised of a PDZ domain, actin-interacting domains, a coiled-coil domain, and a GTPase-activating protein (GAP) domain specific to the Rap family of small GTPases. SIPA1L1 was shown to possess actin-reorganizing activity through its actin-interacting domains and that it promotes dendritic spine growth in cultured neurons (thus the name Spine-associated RapGAP, SPAR; Pak et al., 2001). It was further reported that SIPA1L1 is bound and phosphorylated by Polo-like kinase 2 (Plk2) and targeted for degradation by the ubiquitin-proteasome pathway (Pak and Sheng, 2003). Plk2-dependent degradation of SIPA1L1 is suggested to underlie the molecular mechanism of synaptic scaling (Seeburg et al., 2008). Degradation of SIPA1L1 and the resulting weakening of synapses is postulated to accompany shrinkage of dendritic spines and reduction of the number of surface AMPA-Rs and to operate as a part of the small GTPase Ras and Rap signaling regulatory system in homeostatic synaptic plasticity (Lee et al., 2011).

SIPA1L1 was also shown to bind other proteins, including EphA4 receptor and the leucine zipper tumor suppressor (LZTS) family of proteins. EphA4 binds the PDZ domain of SIPA1L1 and is involved in neuronal cell adhesion or axonal growth cone morphogenesis through regulation of Rap1 activity (Richter et al., 2007). The LZTS family of proteins bind SIPA1L1 via a reciprocal coiled-coil domain interaction (Wendholt et al., 2006; Schmeisser et al., 2009). LZTS1/PSD-Zip70 has been suggested as critical for spine localization of SIPA1L1, collaborating with SIPA1L1 in spine maturity and maintenance (Maruoka et al., 2005).

Spinophilin (also known as neurabin-2/PP1R9B) and its paralog, neurabin-1/PP1R9A, are F-actin-binding proteins enriched in dendritic spines (Allen et al., 1997; Nakanishi et al., 1997; Satoh et al., 1998). Spinophilin and neurabin-1 share similar domain structures, which comprise an F-actin-binding domain, a protein phosphatase 1-binding domain, a PDZ domain, and coiled-coil domains. A notable feature of this family of proteins is their ability to modulate G-protein-coupled receptor (GPCR) signaling, which controls various physiological responses. The major difference between the two proteins is their binding and regulatory specificity for GPCRs via their variable receptor-binding domains. To date, spinophilin has been shown to target α_1-adrenergic and α_2-adrenergic receptors (αARs; Wang et al., 2004), muscarinic-acetylcholine receptors (mAchRs; Fujii et al., 2008), dopamine D2 receptors (Smith et al., 1999), μ-opioid receptors (Charlton et al., 2008), and group 1 mGluRs (Di Sebastiano et al., 2016), whereas neurabin-1 targets adenosine A1 receptors (Chen et al., 2012).

Despite various important roles suggested for SIPA1L1 in neurons, its physiological role remains to be investigated. Here, we examined localization of SIPA1L1 in mature mouse brain using super-resolution microscopy (SRM) and immunoelectron microscopy (IEM). Unexpectedly, we found that SIPA1L1 is generally localized submembranously in somata and neurites of neurons, and in cytoplasm of dendritic spines, but that it is scarce in PSD regions. Screening for native SIPA1L1 interactors in the mouse cerebrum validated spinophilin and neurabin-1, along with other candidate proteins. Finally, we addressed physiological functions of SIPA1L1 by histologic, electrophysiological, pharmacological, and behavioral analyses of *Sipa1l1*$^{-/-}$ mice. The results suggested a critical role of SIPA1L1 in certain types of GPCR signaling and in brain functions that are highly relevant to neuropsychiatric disorders.

Materials and Methods

Antibodies

Polyclonal anti-SIPA1L1, SIPA1L2, and SIPA1L3 antibodies were prepared by immunizing rabbits with fragments of SIPA1L1 (amino acids 1617–1804 of accession no. NP_056371.1), SIPA1L2 (amino acids 1–70 of accession no. NP_065859.3) or SIPA1L3 (amino acids 1049–1251 of accession no. NP_055888.1) fused to glutathione S-transferase. Antibodies were purified by affinity chromatography using columns to which antigens used for immunization had been linked. Other antibodies and reagents used in this work are listed in Table 1.

Targeted disruption of the Sipa1l1 *gene*

Genomic clones for the *Sipa1l1* locus were isolated by screening with a C57BL/6N male liver genomic library (Clontech). The targeting vector was constructed by inserting a nuclear localization signal-*LacZ*-poly A cassette, followed by a *PGK-neo*-poly A cassette at the first methionine site, preserving 0.8 kb (5′) and 5.2 kb (3′) of the flanking regions (Fig. 1*A*). TT2 ES cells were electroporated and selected by standard procedures. Correctly targeted clones were screened by PCR and subsequently confirmed by Southern blotting. Targeted clones were used for aggregation with eight-cell embryos, and chimeric males were mated with C57BL/6N females. Subsequent genotyping was performed by genomic PCR. Primers used were forward: 5′-TAGATCCGTGTGCCACAA-3′, reverse: 5′-GAGGCCAATCTGCTATTC-3′, and LacZ: 5′-CAGTCAC GACGTTGTAAAAC-3′. Heterozygotes were then backcrossed to C57BL/6N mice for at least nine generations. Two- to four-month-old male mice were used for all experiments. They were kept on a 14/10 h light/dark cycle in a temperature-controlled and humidity-controlled (22–24°C, 50–60%) specific pathogen-free vivarium, and they had *ad libitum* access to food and water. All animal experiments were conducted according to guidelines for care and use of animals, approved by the Animal Experiment Committee of the Institute for Quantitative Biosciences, The University of Tokyo and the Okinawa Institute of Science and Technology. License numbers for animal experiments are 23008, 24008, 2514, 2604, 2703, 2801 for the University of Tokyo and 2016-139, 2019-236 for the Okinawa Institute of Science and Technology.

Immunohistochemistry and X-Gal staining

Mice were deeply anesthetized with 90 mg/kg sodium pentobarbital and were intracardially perfused with ice-cold sodium phosphate buffer (pH 7.3, NPB), followed by ice-cold 4% PFA/NPB. Whole brains were removed, separated bilaterally at the medial line, and fixed in ice-cold 4% PFA/NPB for 2 h. Brains were further infiltrated sequentially with 10%, 15%, and 20% sucrose/NPB for >4 h at each concentration and then frozen in a Tissue-Tek OCT compound (Sakura Finetek); 10-μm cryosections were attached to an MAS-coated glass slide (S9441 Matsunami) and air dried for 2 h. For permeabilization, sections were incubated in 0.3% Triton X-100/Tris-buffered saline (pH 7.5; TBS) for 10 min at room temperature (RT) except for synaptophysin and spinophilin (mouse antibody) staining. Alternatively, sections were incubated in 0.4 mg/ml pepsin in 0.2 N HCl for 2 min at 37°C for a PSD localization assay. For synaptophysin and spinophilin (mouse antibody) staining, sections were incubated in boiling 10 mM sodium citrate for 5 min. Sections were blocked with TBS containing a 0.5% blocking reagent (Roche), 2% fetal bovine serum, and 0.1% Tween 20 for 1 h. Then they were incubated overnight at 4°C with primary antibodies diluted in the blocking buffer. In the case of reactions containing mouse antibodies, reagents from the VECTOR M.O.M. Basic kit (Vector Laboratories) were added. After washes in TBS containing 0.1% Tween 20 (TBST), sections were incubated for 1 h at RT with secondary antibodies diluted in blocking buffer. Sections were subsequently stained with TOPRO-3 or DAPI, washed, and coverslipped with Vectashield mounting medium (Vector Laboratories). Sections from wild-type (WT) and knock-out (KO) mice were processed simultaneously on the same slide glass. Antibodies and their dilutions used for immunostaining are listed in

Table 1. Antibodies and reagents

Antigen	Source	Identifier	Host (clone)	Working dilution (x-fold) WB	IHC/ICC
Primary antibodies					
α-Actinin-1	Sigma-Aldrich	A5044	MmAb (BM-75.2)	500	80
Bassoon	Novus Biologicalals	NB120-13249	MmAb (SAP7F407)	–	100
Clathrin HC	BD Transduction	610500	MmAb (23)	1000	40
DAP (GKAP, SAPAP)	NeuroMab	N127/31	MmAb (N127/31)	20	10
Drebrin	MBL	D029-3	MmAb (M2F6)	1000	20
EphA4	Invitrogen	37-1600	MmAb (4C8H5)	250	–
FLAG	Sigma-Aldrich	F3165	MmAb (M2)	5000	300
FLAG	MBL	PM020	RpAb	1000	
GAD67	Chemicon	MAB5406	MmAb (MAB5406)	–	100
GFAP	NeuroMab	N206A/8	MmAb (N206A/8)	–	25
GluA1	Chemicon	AB1504	RpAb	–	40
GluA2	Millipore	AB1768-I	RpAb	–	200
GluN1	BD Pharmingen	556308	MmAb (54.1)	500	200
GluN2B	BD Transduction	N38120	MmAb (13)	500	40
LZTS1	BD Transduction	611710	MmAb (1/FEZ1)	250	–
LZTS2	Santa Cruz Biotechnology	sc-271958	MmAb (B-5)	100	–
LZTS3	Santa Cruz Biotechnology	sc-85844	GpAb	250	–
MAP2	Sigma-Aldrich	M4403	MmAb (HM2)	–	80
Myc	MBL	M192-3	MmAb	1000	
Na^+, K^+ -ATPase α3	Santa Cruz Biotechnology	sc-16052	GpAb	1000	40
Na^+, K^+ -ATPase α3	Santa Cruz Biotechnology	sc-58631	MmAb (XVIF9-G11)	–	40
NeuN	Millipore	ABN78	RpAb	–	100
Neurabin-1	Santa Cruz Biotechnology	sc-32932	RpAb	250	80
Neurexin-1/2/3	Synaptic Systems	175003	RpAb	250	–
Neuroligin-1	R&D Systems	AF4340	SpAb	200	–
Neuroligin-3	R&D Systems	AF6088	SpAb	–	20
PSD-95	UPSTATE	05-494	MmAb (K28/43)	1500	–
PSD-95	Abcam	ab12093	GpAb	–	40
SIPA1L1	See Materials and Methods	–	RpAb	1500	80
SIPA1L2	See Materials and Methods	–	RpAb	500	20
SIPA1L3	See Materials and Methods	–	RpAb	2000	80
Spinophilin	Abnova	H00084687-A01	MpAb	–	40
Spinophilin	Santa Cruz Biotechnology	sc-14774	GpAb	500	40
Synapsin1/2	Synaptic Systems	106 004	GupAb	–	200
Synaptophysin	Sigma-Aldrich	S5768	MmAb (4C8H5)	–	40
SynGAP	Santa Cruz Biotechnology	sc-8572	GpAb	250	–
α-Tubulin	Calbiochem	CP-06	MmAb (DM1A)	500	–
β-Galactosidase	Promega	Z3781	MmAb	–	500
Secondary antibodies and reagents					
Rabbit anti-sheep IgG H&L (HRP)	Abcam	ab6747	–	2000	–
Donkey anti-goat IgG-HRP	Santa Cruz Biotechnology	sc-2033	–	5000	–
Donkey anti-rabbit IgG-HRP	GE Healthcare	NA934	–	10,000	–
Sheep anti-mouse IgG-HRP	GE Healthcare	NA931	–	10,000	–
Goat anti-mouse IgM-HRP	Santa Cruz Biotechnology	sc-2064	–	2000	–
Alexa Fluor 405 goat anti-mouse IgG	Molecular Probes	A48255	–	–	200–400
Alexa Fluor 488 goat anti-rabbit IgG	Molecular Probes	A-11008	–	–	200–400
Alexa Fluor 594 goat anti-mouse IgG	Molecular Probes	A-11005	–	–	200–400
Alexa Fluor 488 donkey anti-rabbit IgG	Molecular Probes	A-21206	–	–	200–400
Alexa Fluor 488 donkey anti-mouse IgG	Molecular Probes	A-21202	–	–	200–400
Alexa Fluor 594 donkey anti-goat IgG	Molecular Probes	A-11058	–	–	200–400
Alexa Fluor 488 goat anti-mouse IgM	Molecular Probes	A-21042	–	–	200–400
Alexa Fluor 647 donkey anti-rabbit IgG	Molecular Probes	A-31573	–	–	200–400
Alexa Fluor 647 donkey anti-mouse IgG	Molecular Probes	A-31571	–	–	200–400
Alexa Fluor 647 donkey anti-guinea pig IgG	Molecular Probes	A-21450	–	–	200–400
Alexa Fluor 546 donkey anti-sheep IgG	Molecular Probes	A-21098	–	–	200–400
Alexa Fluor Plus 555 Phalloidin	Molecular Probes	A30106	–	–	40
TO-PRO-3	Molecular Probes	T3605	–	–	5000

R, rabbit; M, mouse; G, goat; S, sheep; Gu, guinea pig; pAb, polyclonal antibody; mAb, monoclonal antibody. MpAb (Abnova) and GpAb (SantaCruz) for spinophilin, which were raised against different regions of spinophilin, gave similar results when double stained with SIPA1L1. MmAb (SantaCruz) and GpAb (SantaCruz) for Na^+, K^+ -ATPase α3, which were raised against different immunogens, gave similar results when double stained with SIPA1L1. The GpAb for spinophilin was used for pepsin-pretreatment analysis to unify the permeabilization method with the rest of other antibodies in the nontreatment condition.

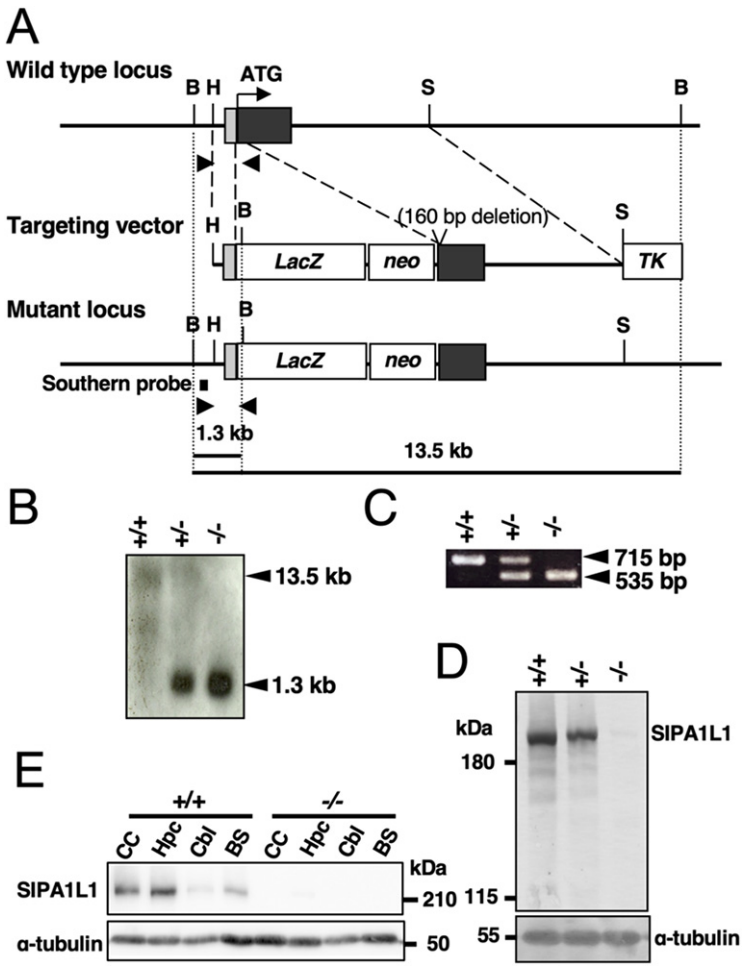

Figure 1. Targeted disruption of the *Sipa1l1* gene. ***A***, A restriction map. Coding and noncoding regions in exons are indicated by black and gray boxes, respectively. Arrowheads indicate primer positions used in PCR genotyping. B, BamHI; H, HindIII; S, SphI; LacZ, β-galactosidase gene; neo, neomycin resistance gene; TK, herpes simplex virus thymidine kinase. ***B***, Southern blot analysis of genomic DNA extracted from mouse tail. Genomic DNA was digested with BamH I. The expected 13.5-kb (WT locus) and 1.3-kb (targeted locus) fragments were generated. ***C***, Genotyping of progeny of *Sipa1l1*+/— intercrosses by PCR. ***D***, ***E***, Western blot analysis of the whole-brain (***D***) or region-specific (***E***) lysate from mature mice. BS, brainstem; Cbl, cerebellum; CC, cerebral cortex; Hpc, hippocampus; kDa, kilodalton.

Table 1. A Zenon Rabbit IgG Labeling kit (Invitrogen) was used for staining neurabin-1 according to manufacturer's instructions. Briefly, labeling of SIPA1L1 was performed following a regular protocol as above until secondary antibody incubation. After TBST washes, sections were incubated with Zenon-labeled (molar ratio 6:1) neurabin-1 antibody for 1.5 h at RT. After three TBST and two PBS washes, sections were fixed with 4% PFA for 15 min, washed, and coverslipped with Vectashield mounting medium. A parallel experiment using negative-control omitting neurabin-1 antibody in the Zenon labeling reaction resulted in no significant signal. For diaminobenzidine (DAB) staining, Vectastain Elite ABC and Avidin/Biotin Blocking kits (Vector Laboratories) were used in conjunction with the above procedures. For X-Gal staining, dried sections were stained overnight at 37°C in an X-Gal staining solution and subsequently counterstained with Nuclear Fast Red (Vector Laboratories). Nissl staining was performed by incubating sections in a 1% thionin solution for 60 min at RT. Digital images were obtained using commercial Olympus microscopes. Briefly, low magnification images were obtained with an IX-83 (Olympus) equipped with a DP80 camera and a motorized stage using a 20× objective. Whole-brain sections or regions of interest were scanned and stitched automatically using cellSense software (Olympus). For confocal imaging, either an FV1000 (Olympus) with a 100×, 1.4 NA silicone immersion objective UPLSAPO100XO or a Leica TCS SP8 LIGHTNING confocal microscope equipped with an HC PL APO CS2 20×/0.75 DRY objective, motorized stage, and LAS X software was used. For SRM, the SD-OSR (Olympus) equipped with a Yokogawa CSU-W1 scanner, Hamamatsu Orca Flash 4 V2+ High Speed SCMOS camera, and a 100×, 1.35 NA silicone immersion objective with correction collar (UPLSAPO100XS) was used to acquire Z-stack images (200-nm step size, all channels scanned in each plane) of 1024 × 1024 pixels (41 × 41 μm^2)/image. Original images adjusted only for brightness and contrast with Fiji/ImageJ (NIH) are shown in the figures.

IEM

Mice were fixed by transcardial perfusion with 3% glyoxal-based fixative (Richter et al., 2018). Brains were cryoprotected with 30% sucrose in 0.1 M phosphate buffer to prepare 50-µm cryosections on a cryostat (CM1900; Leica Microsystems). All immunohistochemical incubations were performed at RT. For silver-enhanced preembedding immunogold electron microscopy, microslicer sections were dipped in 10% normal goat serum /PBS for 30 min, incubated overnight with SIPA1L1 antibody (1:1000) diluted with 0.1% Triton X-100/PBS, and subjected to silver-enhanced immunogold labeling using anti-rabbit IgG conjugated with 1.4-nm gold particles (Nanogold) and R-Gent SE-EM Silver Enhancement Reagents (Aurion). Sections were further treated with 1% osmium tetroxide and 2% uranyl acetate, and embedded in Epon812. Ultrathin sections (100 nm) were prepared with an ultramicrotome (Leica), and photographs were taken with an H7100 electron microscope (Hitachi). The distribution of immunogold particles was quantitatively analyzed on electron micrographs using MetaMorph software (Mlecular Devices; $n = 2$ mice). Perpendicular distribution of PSD-95 or SIPA1L1 was examined by sampling synaptic profiles whose presynaptic and postsynaptic membranes were cut perpendicularly to the plane of the synaptic cleft, and by measuring the distance from the midline of the synaptic cleft to the center of immunogold particles. Statistical significance was assessed using the Kolmogorov–Smirnov test.

Spine size analysis by electron microscopy

Electron microscopy was basically performed as described (Meng et al., 2002). Briefly, littermate mice (two to three months) were deeply anesthetized with sodium pentobarbital and were intracardially perfused for 5 min with 2.5% glutaraldehyde in a 0.1 M phosphate buffer (pH 7.4). Hippocampi were removed from whole brains, and the CA1 areas of hippocampi were cut into tiny blocks. These blocks were postfixed in the same fixative for 3 h, osmicated with 1% osmium tetroxide in a 0.1 M phosphate buffer for 2 h, washed thoroughly with 5% sucrose, dehydrated in a graded alcohol series, embedded in Epok812 (#02-1001, Okenshoji Co), and cured for 12 h at 60°C. For each block, 1-μm sections were cut and stained with 1% toluidine blue to guide further trimming to isolate the equivalent CA1 subfields. Ultrathin sections (80 nm) were cut with a diamond knife and stained with uranyl acetate and lead citrate, and then observed with a JEOL JEM1010 electron microscope operated at 100 kV. Similar neuropil areas of the stratum radiatum not containing cell bodies or blood vessels were randomly selected within 100–250 μm of the CA1 pyramidal cell body and photomicrographed at 5000× magnification. Five electron micrographs representing 1300- to 1400-μm^2 neuropil regions of each mouse were taken. Image negatives

were scanned at 1200 dpi and analyzed with ImageJ. The number of synapses (synapse density), PSD lengths, and cross-sectional areas of spine heads from four mice per genotype were quantified. Excitatory synapses bearing spines were defined by the presence of a clear PSD facing at least three presynaptic vesicles. Measurements were performed by an experimenter blind to the genotype.

Electrophysiological analysis

Standard procedures and solutions described previously (Kobayashi et al., 2016) were used. In brief, hippocampal slices (400 μm) were prepared from mice 8–12 weeks of age. Synaptic responses were recorded at 25.0 ± 0.5°C with extracellular field-potential recordings in the stratum radiatum of the CA1 region using a glass recording pipette filled with 3 M NaCl. External solution contained the following: 119 mM NaCl, 2.5 mM KCl, 1.3 mM $MgSO_4$, 2.5 mM $CaCl_2$, 1.0 mM NaH_2PO_4, 26.2 mM $NaHCO_3$, 11 mM glucose, and 0.1 mM picrotoxin (a $GABA_A$-receptor antagonist). To evoke synaptic responses, Schaffer collateral/commissural fibers were stimulated at 0.1 Hz (test pulse) with a bipolar tungsten electrode. Stimulus strength was adjusted to evoke EPSPs with a slope of 0.10–0.15 mV/ms, except for experiments examining input-output relationships. Input–output relationships were examined in the presence of a low concentration of the non-NMDA receptor antagonist, 6-cyano-7-nitroquinoxaline-2,3-dione (CNQX: 1 μM) in the external solution to partially block AMPA receptor-mediated EPSPs. This partial blockade enables more accurate measurements since the nonlinear summation of field EPSPs is reduced. EPSPs were evoked with various strengths of stimulation, and data were first sorted by binning fiber volley amplitudes. Then EPSP amplitudes were averaged within each bin. Paired-pulse facilitation was examined in the presence of 25 μM D-(−)−2-amino-5-phosphonopentanoic acid (D-AP5). Paired-pulse stimuli at intervals of 50, 100, and 200 ms were applied every 10 s. An Axopatch-1D amplifier (Molecular Devices) was used to record EPSPs. Data were digitized at 10 kHz and analyzed on-line using pClamp software (Molecular Devices). All values were reported as mean ± SEM. Student's *t* test was used to determine whether there was a significant difference in the means of two datasets. Picrotoxin was purchased from Sigma-Aldrich. D-AP5 and CNQX were purchased from Tocris Bioscience.

Colocalization analysis

Colocalization analysis was performed using GDSC ImageJ plug-in according to the developer's Colocalization User Manual (http://www.sussex.ac.uk/gdsc/intranet/microscopy/UserSupport/AnalysisProtocol/imagej/colocalisation). Briefly, SRM images stained for SIPA1L1 and its candidate interacting-proteins at the neuropil region of Layer V cerebral cortex or hippocampal CA1 area were acquired using Olympus SD-OSR as described above. Four serial Z-stack images (200-nm step size) of 1024 × 1024 pixels (41 × 41 μm^2)/image were processed to define foreground and background using the Otsu method (or the Triangle method for images with relatively low signal-to-noise ratio) using Stack Threshold Plugin. Processed images and raw images were used to calculate the statistical significance of Manders coefficient and Pearson correlation coefficient, respectively, with the confined displacement algorithm Plugin. If the presence of irregular structures such as somata interfered with the analysis, the corresponding region was excluded from the confined region. Random displacement was defined using a radial displacement chart for Pearson correlation coefficient for each sample. A P value of <0.01 was adopted for statistical significance. Raw image data used in the analyses were deposited on Mendeley at https://doi.org/10.17632/f964whtpxh.1.

Cell culture, transfections, immunostaining, and immunoprecipitation (IP)

HEK293T or COS-7 cells were cultured in DMEM supplemented with 10% fetal bovine serum at 37°C, 5% CO_2. Expression vectors for the SIPA1L family of proteins were generated by cloning human *SIPA1L1* (NM_015556.3), *SIPA1L2* (AY168879), or *SIPA1L3* (AY168880) cDNA into FLAG- or Myc-pcDNA3.1 (+). Expression vectors for spinophilin have been described elsewhere (Sagara et al., 2009). Transfections of plasmid constructs were performed using Lipofectamine 2000 (Invitrogen) for HEK293T and Lipofectamine LTX (Invitrogen) or TransIT-LT1 (Mirus Bio) for COS-7 cells, according to manufacturers' instructions. Immunostaining was performed as described previously (Sagara et al., 2009). For IP, COS-7 cells were lysed in lysis buffer (0.33% SDS, 1.67% Triton X-100, 50 mM Tris-HCl pH 7.4, 150 mM NaCl, 1 mM EDTA, 1 mM EGTA, 1 mM PMSF, 1 mM Na_3VO_4, 25 mM NaF, 5 μg/ml aprotinin, chymostatin, leupeptin and pepstatin A, 10% glycerol), rotated for 60 min at 4°C and centrifuged at 17,000 × *g* for 40 min. Supernatants were precleared with Dynabeads Protein G (Invitrogen Dynal) and incubated with anti-Myc (MBL) antibody-bound Dynabeads Protein G with overnight rotation at 4°C. Samples were then washed four times with wash buffer (0.33% SDS, 1.67% Triton X-100, 50 mM Tris-HCl pH 7.4, 150 mM NaCl, 1 mM EDTA, 1 mM EGTA, 10% glycerol). Proteins were eluted by incubation in 50 mM Tris, pH 6.8 with 2% SDS for 10 min at RT with shaking. Samples were analyzed by Western blotting (WB), as above.

Crosslinking IP combined with mass spectrometry (cIP-MS) and cIP-Western blotting (cIP-WB) analyses

Mouse brain regions of interest were quickly dissected on a filter paper soaked with ice-cold homogenization buffer (HB; 0.32 M sucrose, 20 mM HEPES pH 7.4, 1 mM EDTA, 1 mM EGTA, 5 mM NaF, and 1 mM Na_3VO_4) and were homogenized in ice-cold HB using a Dounce homogenizer. After homogenates were centrifuged at 800 × *g* for 10 min, supernatants were transferred to new tubes, and proteins were crosslinked by adding 20 mM DSP (dithiobis [succinimidylpropionate], Thermo Scientific Pierce), a primary amine-reactive and membrane-permeable crosslinker with a 1.2 nM spacer arm, to a final concentration of 200 μM. For noncrosslinked controls, the same volume of solvent (DMSO) was added. Tubes were rotated at 4°C for 10 min, and 1 M Tris-Cl (pH 7.4) was added to a final concentration of 100 mM to terminate the crosslinking reaction. After 15 min of rotation, tubes were centrifuged at 9200 × *g* to obtain the P2 fractions, containing crude synaptosomes and plasma membranes. P2 pellets were solubilized in lysis buffer (2% SDS, 50 mM Tris-HCl pH 7.4, 150 mM NaCl, 1 mM EDTA, 1 mM EGTA, 1 mM PMSF, 1 mM Na_3VO_4, 25 mM NaF, 5 μg/ml aprotinin, chymostatin, leupeptin and pepstatin A, 10% glycerol) at 37°C for 30 min. Five times the volume of ice-cold neutralization buffer (2% Triton X-100, 50 mM Tris-HCl pH 7.4, 150 mM NaCl, 1 mM EDTA, 1 mM EGTA, 1 mM PMSF, 1 mM Na_3VO_4, 25 mM NaF, 5 μg/ml aprotinin, chymostatin, leupeptin and pepstatin A, 10% glycerol) was added and centrifuged at 17 000 × *g* for 1 h. Supernatants were precleared using Dynabeads Protein G (Invitrogen Dynal) and incubated with anti-SIPA1L1, anti-PSD-95 (Millipore Biotechnology), or control IgG antibody with overnight rotation at 4°C. Samples were then rotated with Dynabeads Protein G for 90 min and washed four times with wash buffer (0.33% SDS, 1.67% Triton X-100, 50 mM Tris-HCl pH 7.4, 150 mM NaCl, 1 mM EDTA, 1 mM EGTA, 10% glycerol). Proteins were decrosslinked and eluted by incubation in a 2× SDS sample buffer containing 200 mM DTT for 60 min at 37°C followed by 10 min at 56°C with constant mixing at 1400 rpm on an Eppendorf ThermoMixer. Dynabeads and unsolubilized materials were carefully removed magnetically and by centrifugation. Final supernatants were analyzed by SDS-PAGE.

For silver staining analysis, Perfect NT Gel (5–20%, DRC Co) was used for SDS-PAGE. Staining and destaining were performed using SilverQuest (Invitrogen), according to the manufacturer's protocol. Selected bands or corresponding areas in control lanes were excised and cut into 1 mm cubes, destained, and reduced with DTT (10 mM in 100 mM NH_4HCO_3, 56°C for 60 min) followed by alkylation with iodoacetamide (55 mM in 100 mM NH_4HCO_3 RT for 45 min). After repeated alternate washings with 100 mM NH_4HCO_3 and acetonitrile, gel pieces were rehydrated with 10 μl 50 mM NH_4HCO_3 containing 25 μg/ml trypsin (Trypsin Gold, Promega) and incubated for 15 min on ice; 10 μl of 50 mM NH_4HCO_3 was added, and trypsin digestion was conducted overnight at 37°C. Peptides were extracted with 20 μL of 20 mM NH_4HCO_3, followed by 20 μl of 50% acetonitrile, 0.1% trifluoroacetic acid (TFA) three times. The volume of pooled supernatants was reduced to 10–20 μl by vacuum centrifugation and then loaded into an automated electrospray ionization (ESI)-MS/MS system, which consisted of the DiNa

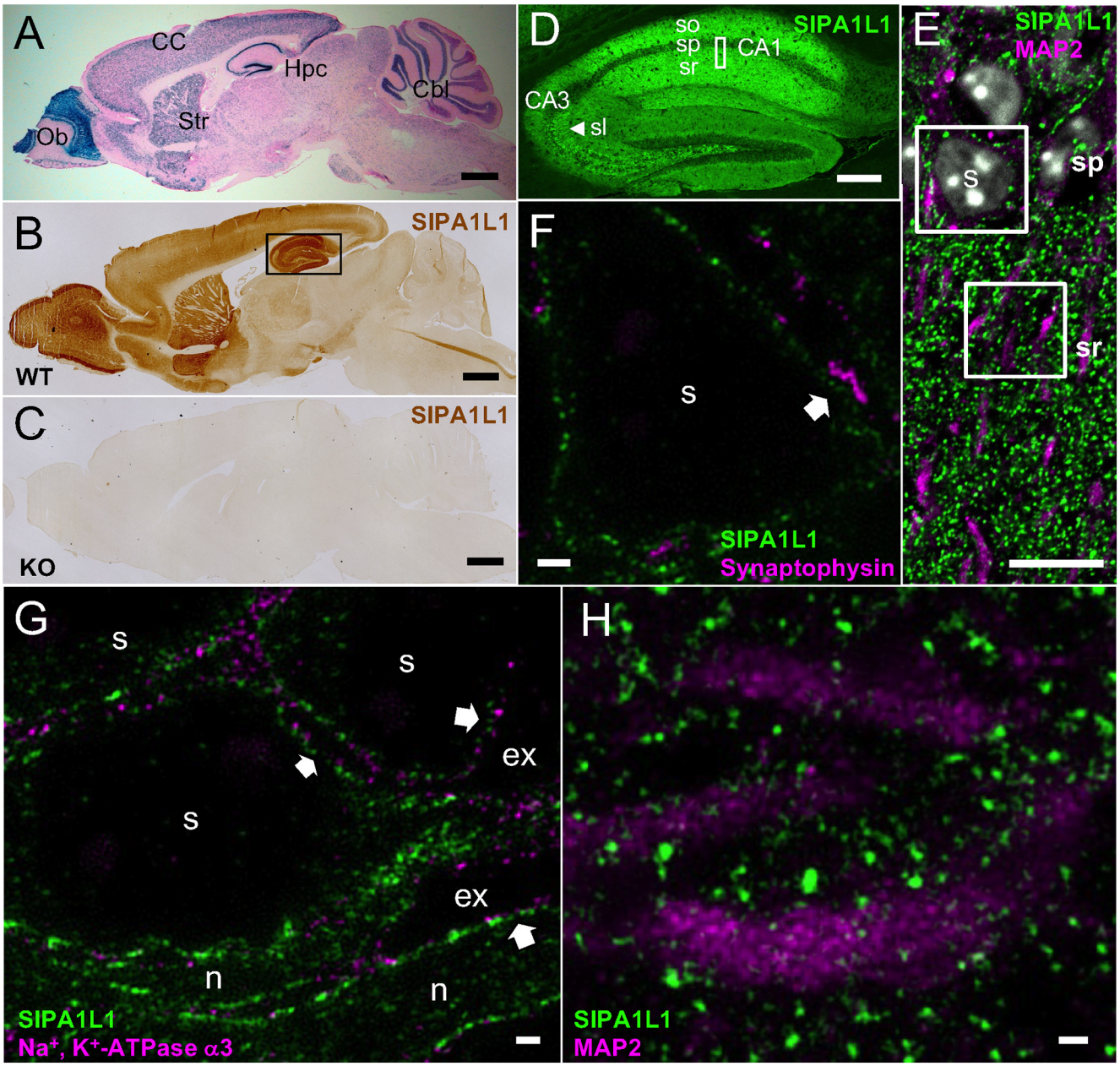

Figure 2. SIPA1L1 localizes to submembranous regions in somata of neurons in mature brain. ***A***, X-Gal staining of *Sipa1l1*+/− brain. ***B–D***, Immunostaining of WT (***B***, ***D***) or *Sipa1l*$^{-/-}$ (***C***) brain using anti-SIPA1L1 antibody. ***D***, Image corresponding to the boxed area in ***B***. ***E–H***, Double immunostaining images of SIPA1L1 and MAP2 (***E***, ***H***), synaptophysin (***F***), or Na^+, K^+-ATPase $\alpha 3$ (***G***). ***E***, Image corresponding to the boxed area in ***D***. Images corresponding to the top (***F***, ***G***) or bottom (***H***) boxed area in ***E***. Note that higher magnification images were obtained independently and are not direct magnifications of boxed areas. Light (DAB staining; ***B***, ***C***), fluorescent (***D***), confocal (***E***), or SRM images (***F–H***), respectively. Arrows in ***F***, ***G*** show examples of submembranous distributions of SIPA1L1. The arrow in ***F*** also indicates a presynaptic terminal represented by synaptophysin. Cbl, cerebellum; CC, cerebral cortex; Hpc, hippocampus; Ob, olfactory bulb; Str, striatum; so, stratum oriens; sp, stratum pyramidale; sr, stratum radiatum; sl, statum lucidum, s, soma; ex, extracellular area; n, proximal neurite. Scale bars: 1000 μm (***A–C***), 200 μm (***D***), 10 μm (***E***), and 1 μm (***F–H***).

system (KYA Tech Corporation) equipped with a C18 ESI capillary column (100 μm × 150 mm, NIKKYO Technos) and an LTQ Velos Orbitrap ETD instrument (ThermoFischer Scientific). For protein identification, spectra were processed using Proteome Discoverer Version 1.2 (ThermoFisher Scientific) against SEQUEST with a 5% false discovery rate (FDR) cutoff. Experiments were performed once each for cerebral cortex and hippocampus. Candidate SIPA1L1-interacting proteins were defined as proteins detected only in WT samples (PSMs ≧ 2) or if PSMs of WT were >10-fold of that of KO samples.

WB was performed by standard methods. Briefly, proteins were transferred to PVDF membranes (Immobilon, Millipore) and 5% skim milk, 0.1% Tween 20 in TBS was used for blocking and antibody dilution. Antibodies and associated dilution factors are listed in Table 1. A chemiluminescent signal was detected using Luminata Forte Western HRP (Millipore) and ImageQuant LAS4000mini (FujiFilm)

GPCR agonist stimulation (sedation) analysis

Nine- to 10-week-old mice were evaluated in the rotarod test for sedation, basically as described previously (Wang et al., 2004). Briefly, the subject was placed on a rotarod (O'hara & Co) rotating constantly at 10 rpm. Mice were trained for three to six sessions until they learned to remain on the rod for 60 s. Mice were injected intraperitoneally with increasing doses of the α_2AR-agonist, UK 14304 (abcam), or the adenosine analog, (-)-N6-(2-Phenylisopropyl) adenosine (R-PIA; Sigma-Aldrich) dissolved in saline. Ten minutes after injection, each mouse was tested three times in succession for its ability to remain on the rotarod.

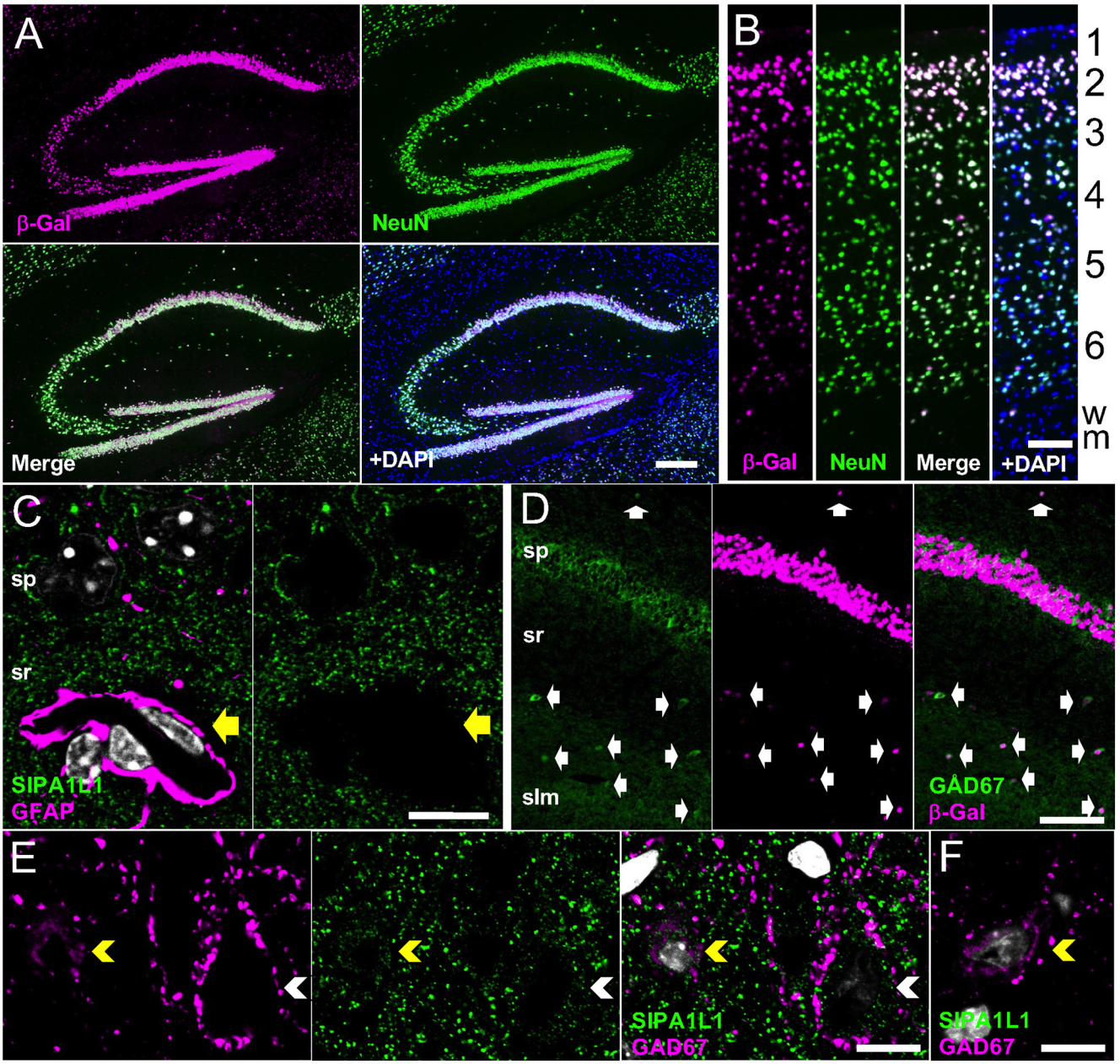

Figure 3. SIPA1L1 is expressed in excitatory and inhibitory neurons but not in glial cells. ***A***, ***B***, Co-staining of β-Galactosidase (β-Gal) and NeuN in mature *Sipa1l1*+/— mouse brain. ***A***, ***B***, Hippocampus and visual cortex, respectively. Nuclear DAPI staining is added in the fourth panels to show the whole population of cells. Numbers on the right indicate layers of visual cortex. wm, white matter. ***C***, GFAP, SIPA1L1, and nuclei (gray) in the hippocampal CA1 region. SIPA1L1 is not detected in GFAP-positive glial cells, indicated by the yellow arrow. ***D***, Co-staining of GAD67 and β-Gal in the *Sipa1l1*+/— hippocampal CA1 region. Arrows show *Sipa1l1* promoter activity in GABAergic neurons. ***E***, ***F***, Co-staining of GAD67 and SIPA1L1 in the WT (***E***) or *Sipa1l1*$^{-/-}$ (***F***) cerebral cortex. Yellow and white arrowheads indicate GAD67-positive and -negative neurons, respectively. SIPA1L1 is expressed in both types of neurons. Note that dotted signals of GAD67 in the neuropil and on the surface of somata are presynaptic terminals of GABAergic neurons. so, stratum oriens; sp, stratum pyramidale; sr, stratum radiatum; slm, stratum lacunosum moleculare. Fluorescent (***A***, ***B***) or confocal (***C–F***) microscopic images. Scale bars: 200 μm (***A***), 100 μm (***B***, ***D***), and 10 μm (***C***, ***E***, ***F***).

Results of the three trials were averaged. Cumulative doses of agonists are shown in the figure. The cutoff time was 60 s. The experimenter was blinded to the genotype during testing.

Seizure susceptibility analysis

Eight- to nine-week-old mice were injected intraperitoneally with 30 mg/kg of kainate (Sigma-Aldrich) or pentylenetetrazole (PTZ; Sigma-Aldrich) dissolved in saline in a volume of 15 ml/kg. For the α_2AR agonist treatment, eight- to nine-week-old mice were injected intraperitoneally with 1 mg/kg of guanfacine (Sigma-Aldrich) dissolved in saline in a volume of 6 ml/kg 30 min before the injection of PTZ. Mice were placed in a clear Plexiglas cage and videorecorded for up to 2 h or the 30-min cutoff time for kainate-induced or PTZ-induced seizures, respectively. Seizures were scored according to the following scale. Phase 1, hypoactivity: a progressive decrease in motor activity until the animal came to rest in a crouched or prone position with the abdomen in full contact with the cage; phase 2, partial clonus: a brief seizure, typically lasting 1 or 2 s, with clonic seizure activity affecting the face, head or forelimbs; phase 3, generalized clonus: the sudden loss of upright posture, whole body clonus involving all four limbs and tail, typically lasting for 30–60 s, followed by a quiescent period; and phase 4, severe generalized tonic-clonic seizure: a continuous loss of upright posture, lying or rolling on the floor, resulting in death from continuous convulsions. When a phase was skipped, the same latency of higher phases was also adopted for the

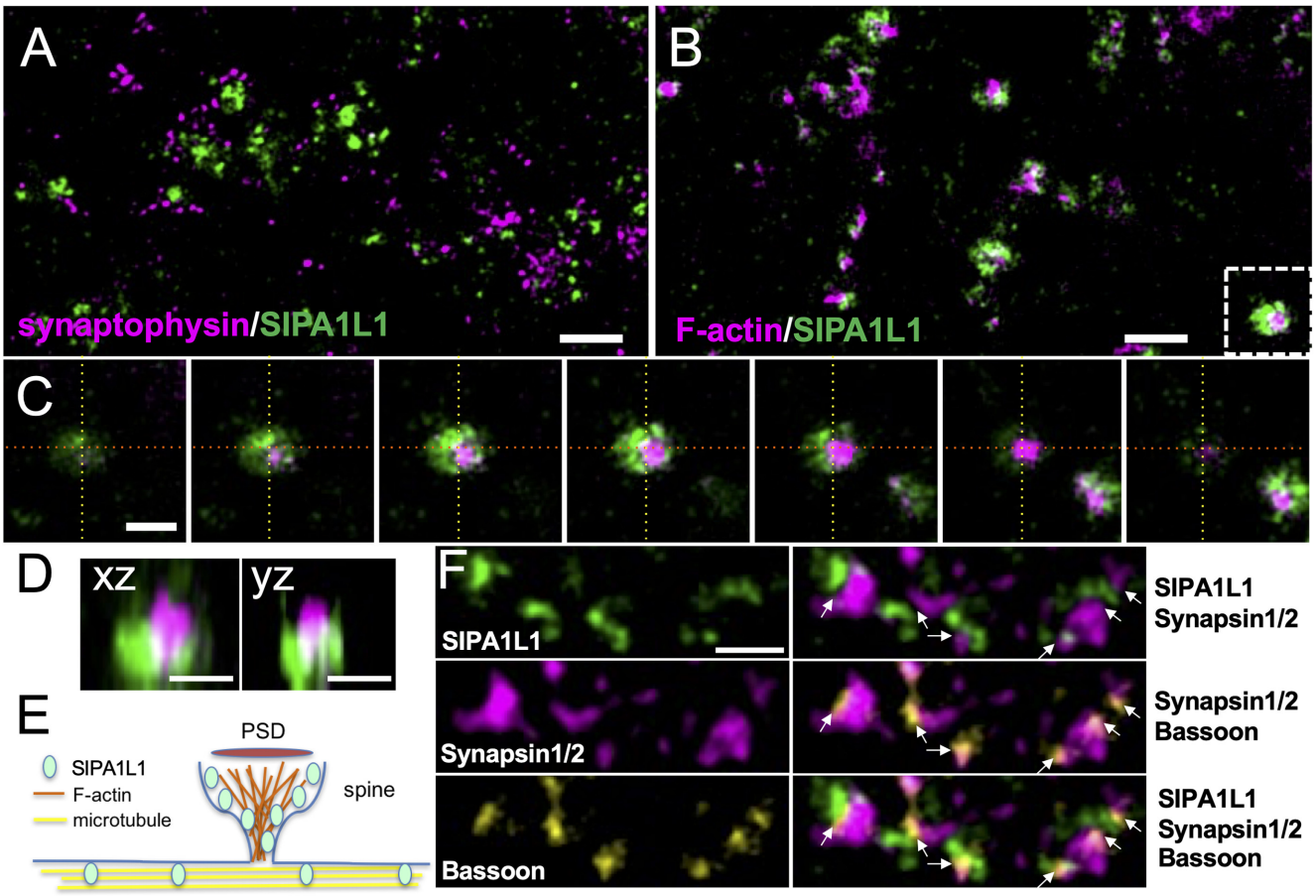

Figure 4. SIPA1L1 localizes postsynaptically in mature neurons in the mouse brain. ***A***, ***B***, Super-resolution immunofluorescence images of SIPA1L1 and synaptophysin (***A***) or F-actin (***B***) in the hippocampal CA3 stratum lucidum. Synaptophysin represents presynaptic vesicles and F-actin is a major cytoskeletal structure in the postsynaptic spine head. ***C***, The dotted boxed area in ***B*** is shown in serial Z-stack images (200-nm step size). ***D***, *XZ* and *YZ* plane images were reconstructed from images in ***C***. Orange and yellow dotted lines in ***C*** indicate the positions of the *XZ* or *YZ* planes, respectively. ***E***, A schematic representation of SIPA1L1 distribution in a dendritic spine. ***F***, Super-resolution immunofluorescence images of SIPA1L1, synapsin1/2, and bassoon in the hippocampal CA3 stratum lucidum. Synapsin1/2 or bassoon represents presynaptic vesicles or presynaptic active zone, respectively. Arrows point to presynaptic active zones between the opposing SIPA1L1 and synapsin1/2 staining. Scale bars: 2 μm (***A***, ***B***) and 1 μm (***C***, ***D***, ***F***).

lower phase. The experimenter was blinded to the genotype during testing.

Behavioral analysis

Male *Sipa1l1*$^{-/-}$ and WT mice were housed together, with two to four littermates (or mice with close birthdays) per cage after weaning. Mice were acclimated to handling and the experimental room for at least 3 d before the start of an experiment. An independent group of mice (two to three months) was used for each test unless otherwise noted. Experimenters were blinded to the genotype during testing. All experiments were analyzed using an automated system from O'hara & Co, except during eyeblink conditioning. All Image series software (O'hara & Co) used for analysis is based on the public domain NIH Image or ImageJ program (https://imagej.nih.gov/nih-image/).

Open field test

Each subject was placed in the center of an open-field apparatus (50 × 50 × 33.3 cm; width × depth × height) illuminated at 20 lux and allowed to move freely for 10 min. Distance traveled in the arena, trace of the movement, rearing activity, and time spent in the center were recorded and analyzed using Image OF 2.15× and Image OFC 2.03sx. Rearing activity was counted manually using the human observation mode of Image OFC 2.03sx. Accelerating rotarod and contextual and cued fear conditioning tests were subsequently performed on the same group of mice with an interval of 2 d between tests.

Accelerating rotarod test

Mice were placed on a rod (3 cm in diameter) rotating at 4 rpm initially, and then the rotation of the rotarod was accelerated linearly to 40 rpm over a 300-s period. Latency to fall off the rotarod during a trial was automatically measured. Mice were trained for two consecutive days, receiving three trials per day at intervals of 90 min between trials.

Light-dark transition test

The apparatus consisted of a box (21 × 42 × 25 cm) divided into two sections of equal size by a partition with a door. One chamber was brightly illuminated (100 lux), whereas the other chamber was dark without illumination. Mice were placed on the dark side and allowed to move freely between the two chambers with the door open for 10 min. The total number of transitions, time spent on each side, latency to enter the light side, and distance traveled were recorded and analyzed automatically using ImageJ LD1.

Morris water maze

A pool 1 m in diameter was filled with opaque water colored with nontoxic white paint and maintained at ~25°C. Each training trial began by placing the mouse in the quadrant that was either right, left, or opposite to the target quadrant containing a submerged platform (10 cm in diameter), in semi-random order. The same order of start positions was used for all subjects. Training trials were a maximum 60 s in duration. A mouse that failed to reach the platform within 60 s was subsequently guided to the platform. Mice that reached or were guided to the platform stayed there for 20 s. Two trials per block with a 1-min intertrial interval,

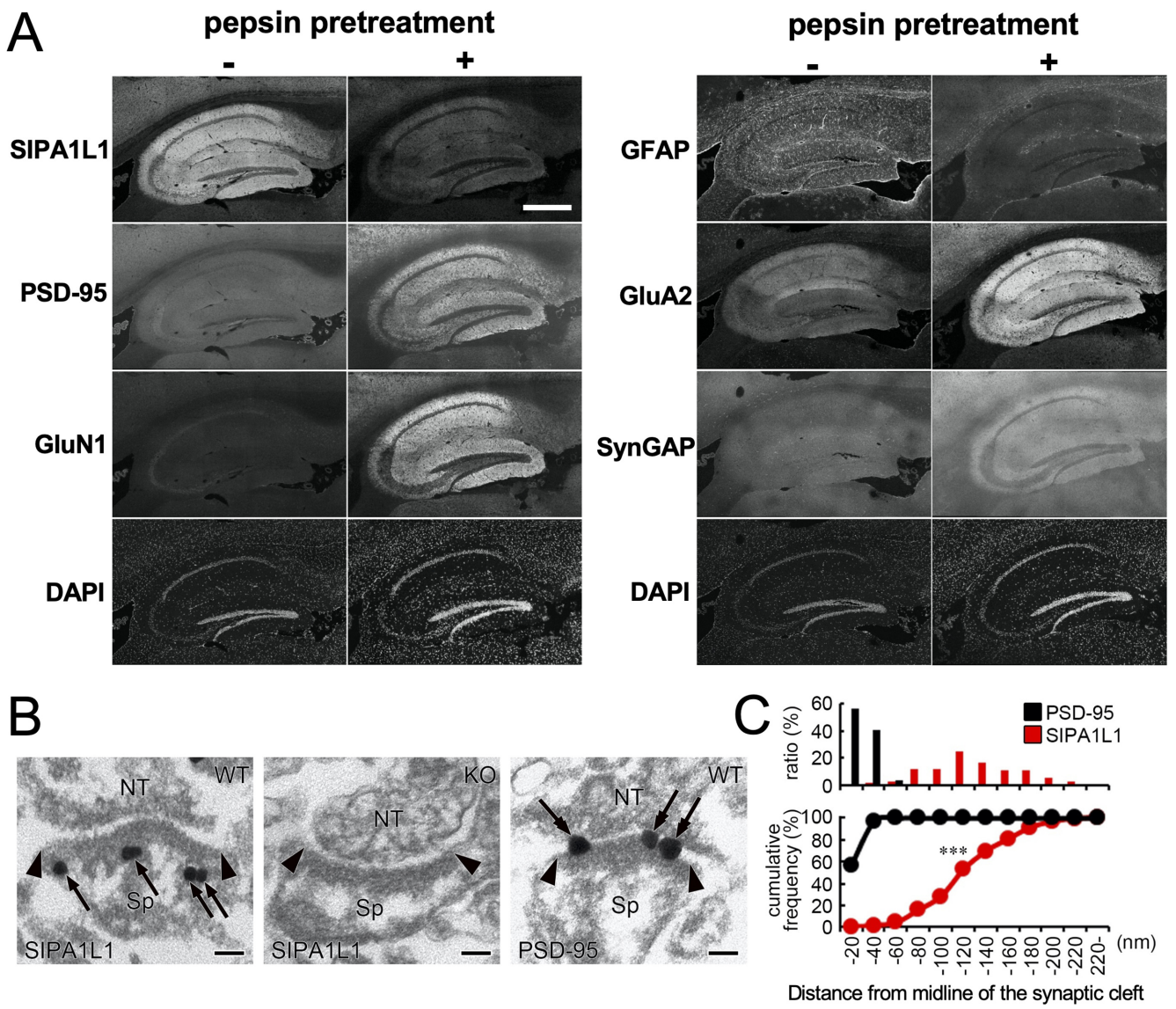

Figure 5. SIPA1L1 localizes to non-PSD regions in dendritic spines. ***A***, Quadruply stained confocal images of hippocampus on indicated proteins and DAPI on pepsin-pretreated (+) or pepsin-untreated (–) brain slices. Paired images are acquired and adjusted with identical settings and conditions. PSD proteins show strong staining with pepsin pretreatment. DAPI staining tends to yield a stronger signal in pepsin-pretreated tissues. ***B***, Electron micrographs of hippocampal CA1 stratum radiatum labeled for SIPA1L1 and PSD-95. *Sipal1*$^{-/-}$ (KO) brain was used as a negative control. Arrows show immuno-metal particles, and arrowheads indicate the extent of PSD. Sp, dendritic spine; NT, presynaptic nerve terminal. ***C***, Distribution of SIPA1L1 and PSD-95 in dendritic spines shown as distance from the midline of the synaptic cleft. Data are in 20-nm bins. A total of 148 and 196 metal particles for SIPA1L1 and PSD-95, respectively, were analyzed. Two tailed Kolmogorov–Smirnov test, $***p < 0.0001$. Scale bars: 500 μm (***A***) and 100 nm (***B***).

three blocks per day with a 1-h interblock interval were conducted for 10 or 5 d to train mice for hidden or visible platform tasks, respectively. The visible platform test was conducted after completion of the hidden platform test. Latency to reach the platform, distance traveled to the platform, and average swim speed were automatically recorded. At the end of the tenth day of hidden platform training, a probe test was conducted for 1 min to confirm that spatial learning had been acquired, based on navigation by distal environmental room cues. Time spent in each quadrant and the number of crossings above the original platform site were automatically recorded. Data were automatically analyzed using Image WM 2.12r, Image WMV 2.08 sr, and Image WMH 2.08s.

Three-chambered social interaction test

Four-month-old mice were used for this social interaction test. The testing apparatus consisted of a rectangular, three-chambered box and a lid with an LED light panel and a CCD monochrome camera. Each chamber was 20 × 40 × 22 cm, and separating walls were made from transparent Plexiglas with small openings (5 × 3 × 3 cm). The subject mouse was first placed in the middle chamber and allowed to habituate to the entire test box for 10 min. After habituation, the mouse was taken out of the box, and an age-matched unfamiliar WT male (stranger mouse), which had no prior contact with the subject mouse, was placed in a small, round wire cage in one of the side chambers. The side on which the stranger mouse was placed was systematically alternated between trials. The subject was placed back in the central chamber for a 10-min session, and the time spent in each chamber, the number of entrances to each chamber, the distance traveled in each chamber or in the periphery of each cage, the total distance traveled, the average travel speed, and the heatmaps were automatically recorded and analyzed using TimeCS1 software (O'hara & Co).

Eyeblink conditioning

Mice were prepared for eyeblink conditioning basically according to previously described procedures (Takatsuki et al., 2003). In brief, under anesthesia with pentobarbital and, if necessary, with diethyl ether inhalation, four Teflon-coated stainless-steel wires (No. 7910, AM Systems)

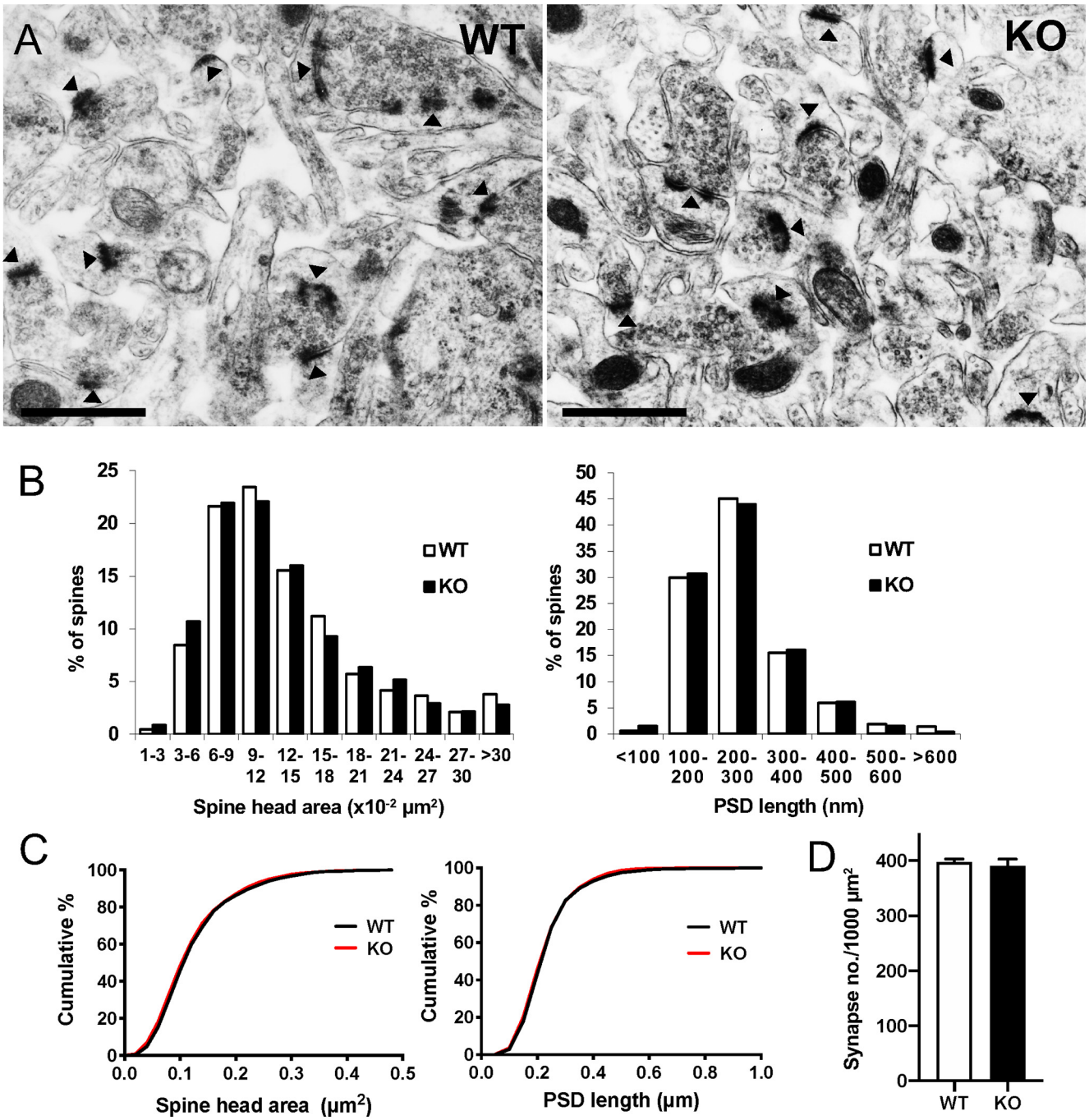

Figure 6. *Sipa1l1*$^{-/-}$ mice show normal synaptic densities and spine size distributions. ***A***, Representative thin-section electron micrographs of hippocampal CA1 stratum radiatum, showing normal asymmetric morphology of synapses in both WT and KO mice. Arrowheads point to PSD in dendritic spines. Scale bar: 1 μm. Frequency (***B***) or cumulative distribution plots (***C***) of cross-sectional spine head area and PSD length. $N = 2110$ (WT) or 2107 (KO) spines from 4 mice per genotype. Two-tailed Kolmogorov–Smirnov test, $D = 0.034$, $p = 0.17$ or $D = 0.030$, $p = 0.29$ for spine head area or PSD length, respectively. ***D***, Synaptic density calculated from same electron micrographs as ***B***, ***C***. In total, 2110 (WT) or 2107 (KO) synapses were analyzed. Mean ± SEM is shown. $t_{(6)} = 0.512$, $p = 0.63$; unpaired two-tailed *t* test.

were implanted under the left upper eyelid. Two of these wires were used to record the eyelid electromyograms (EMGs), and the remaining two delivered an unconditioned stimulus (US). Two to three days after surgery, mice were subjected to 2 d of habituation without US or conditioned stimulus (CS), during which EMGs were recorded to calculate spontaneous eyeblink frequency. Seven or 10 d of delay or trace conditioning, respectively, began the next day. A daily session consisted of 90 CS-US paired trials and 10 CS-alone trials at every 10th trial. The CS was a 350-ms tone (1 kHz, 90 dB) with a 5-ms rise and a 5-ms fall time. The US was a 100-ms periorbital shock (100-Hz square pulses) with the intensity carefully adjusted to elicit a head-jerk response in each animal. The interstimulus interval was 250 or 850 ms in delay or trace conditioning, respectively. Eyelid EMGs were analyzed as described previously (Takatsuki et al., 2003), except that trials that elicited a startle response to the CS were also included for evaluation of conditioned response (CR) occurrence. In brief, the mean ± SD of amplitudes of EMG activity for 300 ms before CS onset in 100 trials was defined as the threshold, which was then used in the analysis below. In each trial, average values of EMG amplitude above the threshold were calculated for 300 ms before CS onset (prevalue), 30 ms after CS onset (startle-value), and 200 ms before US onset (CR-value). If the prevalue was <10% of threshold, the trial was regarded as valid. Among valid trials, a trial was assumed to

contain the CR if the CR value was larger than 1% of the threshold and it exceeded two times the prevalue. For CS-alone trials, the period for CR-value calculation was extended to the CS end. To evaluate the effect on the startle response, we calculated the frequency of trials in which the startle-value exceeded 10% of the threshold.

Experimental design and statistical analyses

All results are expressed as mean ± SEM, unless noted otherwise. Statistical analyses in this work employed unpaired two-tailed Student's *t* tests, two-tailed Welch's *t* tests, two-tailed Mann–Whitney tests, two-tailed Wilcoxon matched pair signed-rank tests, Kolmogorov–Smirnov tests, one-way ANOVA with Geisser–Greenhouse correction followed by Tukey's *post hoc* tests, or a two-way ANOVA with Geisser–Greenhouse correction followed by Sidak's *post hoc* tests, where appropriate, using GraphPad Prism 8. A P value of <0.05 was considered statistically significant. For effect size calculations, Pearson's r or partial η^2 was used. D'Agostino–Pearson test and F tests were used to check normality and equal variance, respectively. More statistical information is available in Extended Data Figure 18-1.

Availability of data and materials

Most of the data generated or analyzed during this study are included in this article and its supplementary information files. Other datasets generated during and/or analyzed during the current study are available from the corresponding authors on request. Most materials are readily available from commercial sources or from our lab. Exceptions are the rabbit polyclonal anti-SIPA1L1, 2, or three antibodies that we generated, or antibodies discontinued from commercial suppliers, because of limited amounts. However, they may be made available for reasonable request.

Results

SIPA1L1 localizes to submembranous regions in neurons but is scarcely associated with PSD

To investigate physiological roles of SIPA1L1, we generated mice lacking *Sipa1l1* (Fig. 1). We first examined the expression pattern and localization of SIPA1L1 in mature brain. *Sipa1l1* promoter activity was present throughout the brain, with the highest activity in the cerebrum, including the hippocampus, cerebral cortex, striatum, and olfactory bulb, in addition to cerebellum (Fig. 2*A*). A strong immunofluorescence signal of SIPA1L1 was detected in WT cerebrum (Fig. 2*B*), mostly consistent with the pattern of *Sipa1l1* promoter activity, with the exception of cerebellum, but not in *Sipa1l1*$^{-/-}$ (KO) brains (Fig. 2*C*). Predominant SIPA1L1 expression in the forebrain was also confirmed by WB (Fig. 1*E*). In the hippocampus, SIPA1L1 immunoreactivity had a relatively stronger signal in the CA1 region, with strong signals in both somata and neuropil regions (Fig. 2*D*,*E*). *Sipa1l1* expression was mostly neuron-specific in the brain, if not neuron-exclusive. (Fig. 3*A*–*C*). SIPA1L1 was not only expressed in excitatory neurons, but also in virtually all GABAergic neurons observed (Fig. 3*D*–*F*).

We next minutely investigated subcellular localization of SIPA1L1, using a confocal-based spinning disk super-resolution microscope, which implements structured illumination microscopy (SIM; Hayashi and Okada, 2015). SIPA1L1 was primarily distributed beneath the plasma membrane in somata and in proximal neurites of pyramidal neurons in the CA1 region (Fig. 2*F*,*G*). SIPA1L1 was relatively evenly distributed, and no specialized structure or distribution was observed in regions apposing presynaptic terminals (Fig. 2*F*). In the neuropil region, co-staining of SIPA1L1 with dendritic marker MAP2 showed large clusters of SIPA1L1 surrounding the dendritic shaft and also smaller signals embedded within the shaft (Fig. 2*H*). Double staining of SIPA1L1 and synaptophysin (Fig. 4*A*) or F-actin (Fig. 4*B*–*E*),

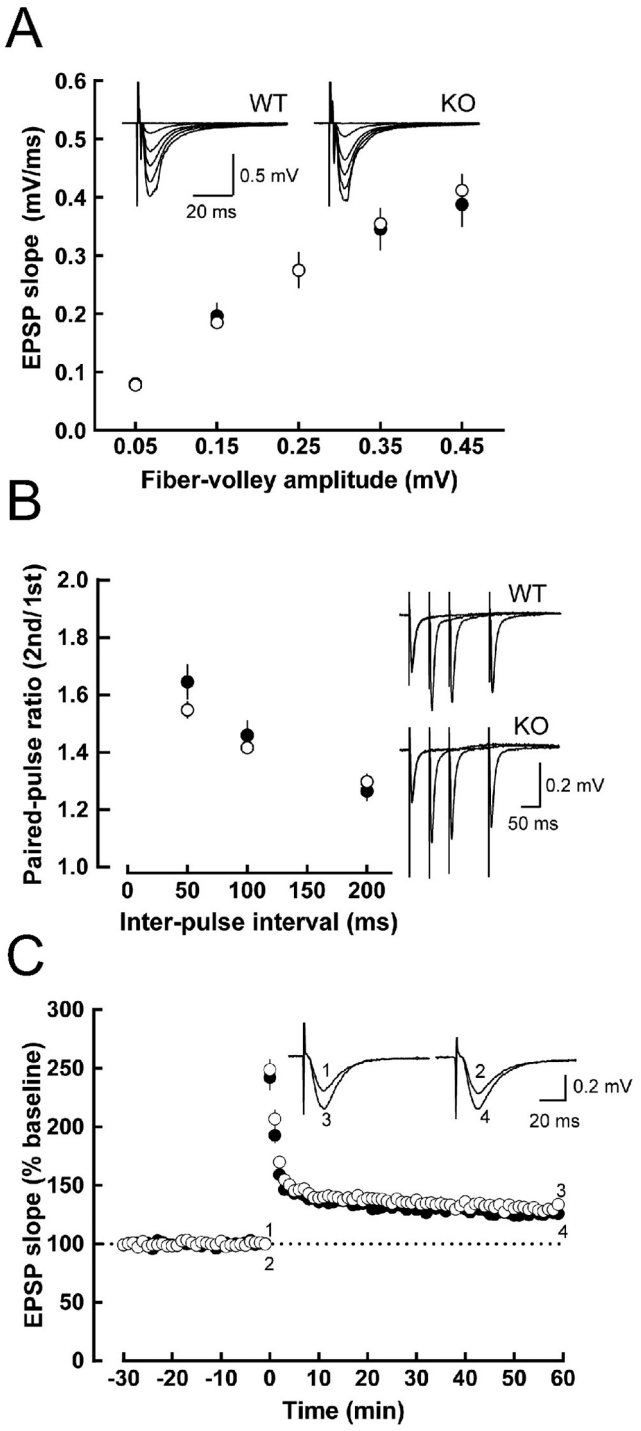

Figure 7. Basal synaptic transmission, paired-pulse facilitation, and hippocampal CA1 LTP are normal in *Sipa1l1*$^{-/-}$ mice. ***A***, The input (fiber-volley amplitude)-output (EPSP slope) relationship of AMPA receptor-mediated EPSPs at Schaffer collateral-CA1 pyramidal cell synapses in acute hippocampal slices of WT (open circles: $n = 10$) and *Sipa1l1*$^{-/-}$ (KO, closed circles: $n = 9$) mice. There was no significant difference between the two genotypes. Sample traces of EPSPs (average of 10 consecutive sweeps) evoked with various stimulus strengths are shown in the inset. ***B***, Paired-pulse facilitation. The paired-pulse ratio (the ratio of slopes of second EPSPs to those of first EPSPs) is shown as a function of interpulse intervals (IPIs) in the presence of 25 mM D-AP5. In any IPI (50, 100, and 200 ms), no significant difference was observed between WT (open circles, $n = 6$ slices) and *Sipa1l1*$^{-/-}$ (closed circles, $n = 6$ slices) mice. Right panel, Sample traces of synaptic responses evoked by paired stimuli at intervals of 50, 100, and 200 ms are superimposed. ***C***, The time course of LTP induced by tetanic stimulation in WT (open circles, $n = 13$ slices) and *Sipa1l1*$^{-/-}$ (closed circles, $n = 12$ slices) mice. A train of high-frequency stimuli (100 Hz, 1 s) was delivered at time 0. Sample traces (average of 10 consecutive responses) in the inset were EPSPs obtained at times indicated by the numbers in the graph.

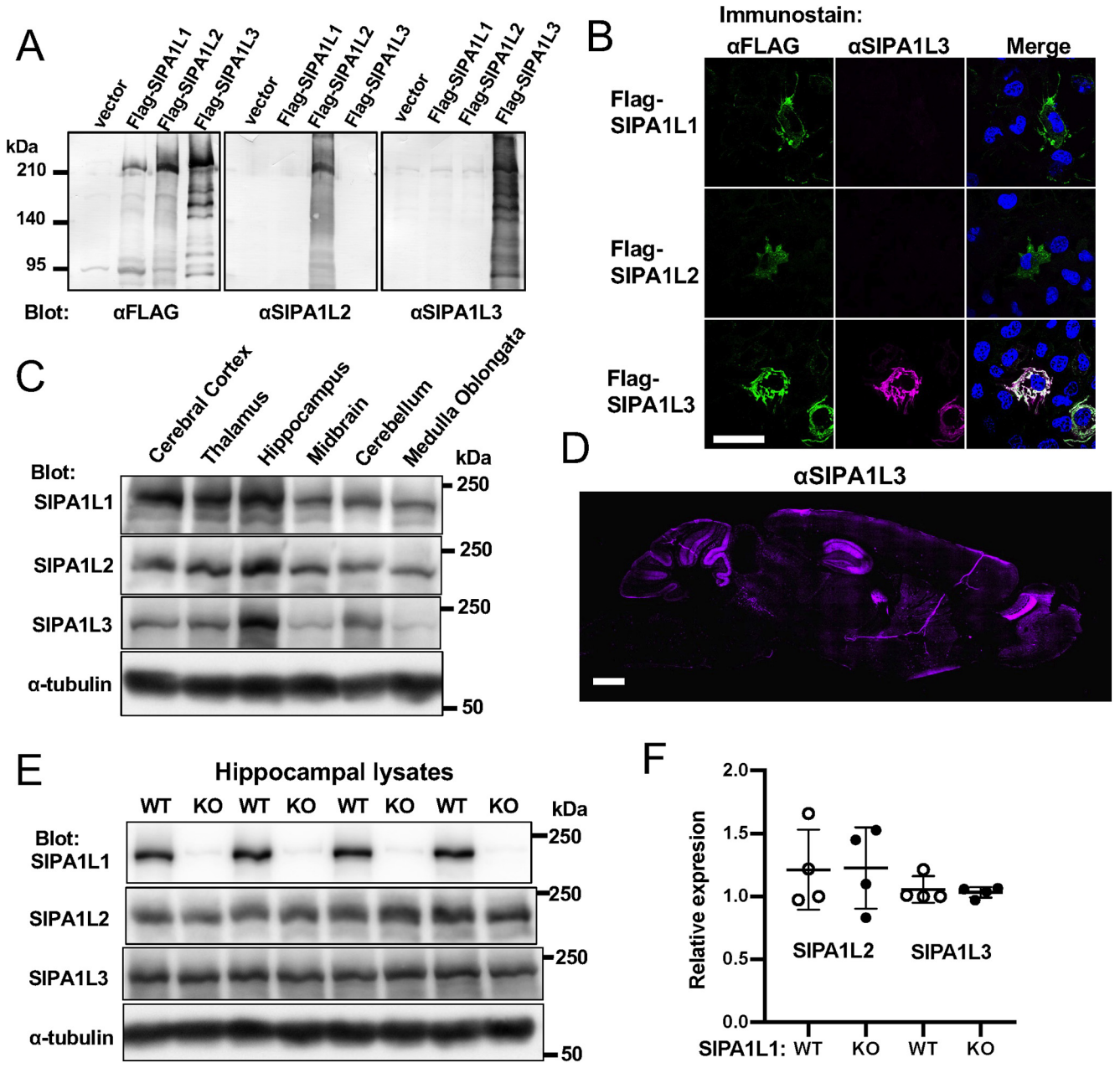

Figure 8. No significant upregulation of SIPA1L1 paralogs in *Sipa1l1*$^{-/-}$ hippocampus. ***A***, ***B***, Validation of anti-SIPA1L2 and anti-SIPA1L3 antibodies by immunoblotting (***A***) and immunostaining (***B***). The indicated FLAG-tagged SIPA1L family proteins were exogenously expressed in HEK293T (***A***) or COS-7 (***B***) cells. Anti-SIPA1L2 and anti-SIPA1L3 antibodies did not cross react with other paralogs. ***C***, Lysates of indicated regions of mature WT brain were subjected to immunoblotting. ***D***, Immunofluorescence staining of SIPA1L3 on sagittal sections from WT brain. SIPA1L2 was not detectable by immunostaining of mouse brain. ***E***, WT and KO hippocampal lysates from littermate pair were placed side by side for immunoblotting. ***F***, Quantification of ***E***, mean ± SD is shown. $N = 4$. $t_{(3)} = 0.113$, $p = 0.92$ for SIPA1L2 and $t_{(3)} = 0.419$, $p = 0.70$ for SIPA1L3; paired two-tailed *t* test. Scale bars: 500 μm (***B***) and 1000 μm (***D***).

and triple staining of SIPA1L1, bassoon and synapsin-1/2 (Fig. 4*F*) in the neuropil region confirmed the generally postsynaptic localization of SIPA1L1 (also see Fig. 12; Extended Data Fig. 15-1). SIPA1L1 and F-actin showed closely associated staining, with SIPA1L1 occasionally surrounding the large actin cytoskeletal structure in dendritic spines (Hotulainen and Hoogenraad, 2010). SIPA1L1 staining tends to decrease as the diameter of inverted conical F-actin structures increases, and little signal was detected near the maximum diameter, where PSD is likely to form (Fig. 4*C*,*D*).

We further investigated whether SIPA1L1 localizes to PSD. It has been shown that conventional immunostaining methods fail to show the true distribution of PSD proteins in brain tissue because of the densely packed nature of PSD, so unmasking of epitopes such as by protease pretreatment is required (Fukaya and Watanabe, 2000). Accordingly, representative PSD proteins, such as PSD-95, NMDA-R subunit GluN1, AMPA-R subunit GluA2, and SynGAP all showed strong specific staining only after pepsin pretreatment. However, SIPA1L1 and the non-PSD protein, glial fibrillary acidic protein (GFAP), showed strong staining without antigen unmasking, and their signals decreased significantly after pepsin pretreatment (Fig. 5*A*). This result suggested that a significant proportion of SIPA1L1 is not associated with PSD. Rather, it localizes to regions to which antibodies and pepsin have easy access, resulting in facilitated detection in pepsin-untreated condition or facilitated degradation in pepsin-

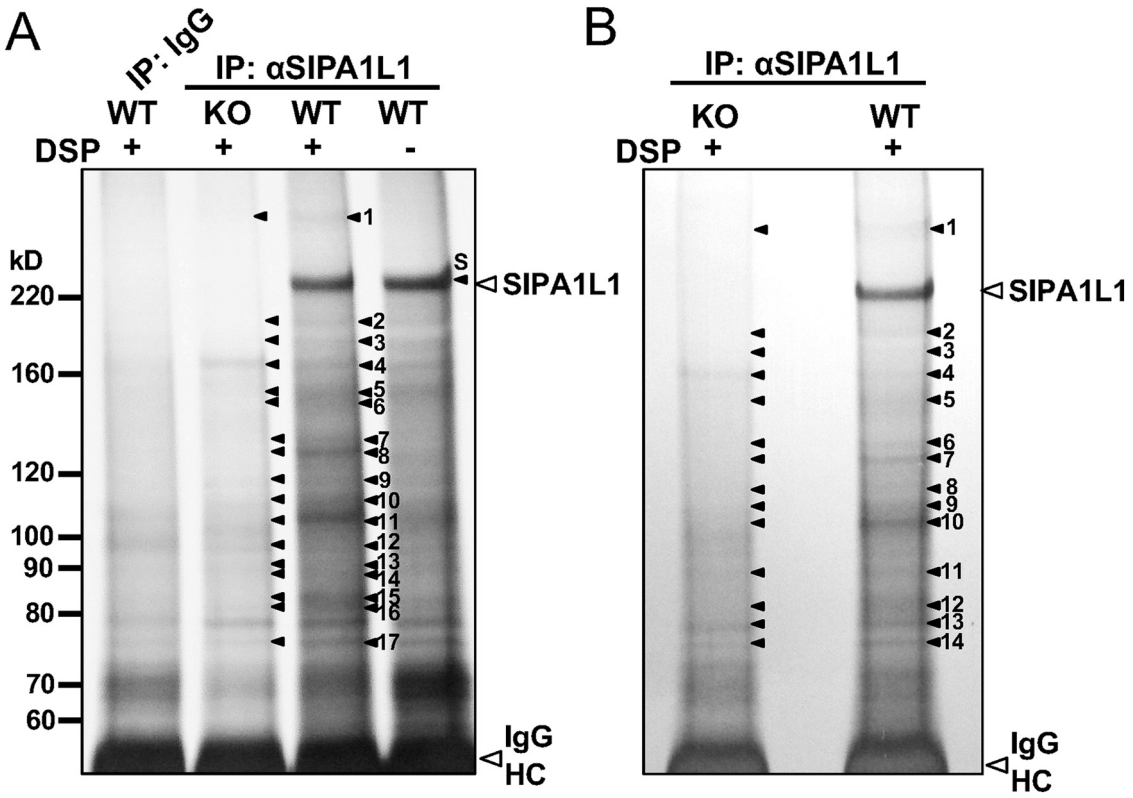

Figure 9. Identification of native interactors of SIPA1L1 by cIP-MS. ***A***, ***B***, Silver staining analysis of an SDS-PAGE gel showing the recovery of proteins co-precipitated with SIPA1L1 or IgG controls from cerebral cortex (***A***) or hippocampus (***B***) lysate. Note bands specific for SIPA1L1 expression and DSP crosslinking. Specific bands in the crosslinked WT (DSP +) lanes and corresponding areas in the SIPA1L1 KO lanes were excised and subjected to LC-MS/MS analyses (Extended Data Fig. 9-1). Arrowheads point to bands excised and numbers or a letter correspond to the Band IDs in Extended Data Figure 9-1.

pretreated condition. To confirm this result, we performed IEM in the hippocampal CA1 neuropil region, using *Sipa1l1*$^{-/-}$ brain tissue as a negative control. In electron micrographs, PSD is defined as an electron-dense structure extending 30–50 nm into the cytoplasm beneath the postsynaptic membrane. Accordingly, PSD-95 staining showed distribution mostly within 40 nm of the midline of the synaptic cleft. However, SIPA1L1 staining showed a broad distribution within 60–200 nm from the midline of the synaptic cleft, peaking around 120 nm, but with sparse staining 0–60 nm (Fig. 5*B*,*C*). This showed striking contrast to DAP/GKAP, a protein that binds directly to PSD-95 at the same domain that binds SIPA1L1. DAP/GKAP showed a clear peak within the PSD area by IEM (Valtschanoff and Weinberg, 2001). These results indicated that at least a vast majority of SIPA1L1 is not in close proximity to PSD-95, as would occur in direct binding.

These mostly submembranous and non-PSD localizations of SIPA1L1 suggest a more general and/or extrasynaptic function of SIPA1L1 in neurons, which has not been appreciated.

Sipa1l1$^{-/-}$ mice show normal spine size distribution and NMDA-R-dependent synaptic plasticity

As exogenous SIPA1L1 expression was shown to promote spine head growth (Pak et al., 2001), and its Plk2-dependent degradation is thought to result in spine shrinkage in hippocampal neuronal cultures (Seeburg et al., 2008; Lee et al., 2011), we examined the change in cross-sectional areas of spine heads and PSD lengths in the CA1 stratum radiatum of *Sipa1l1*$^{-/-}$ hippocampus, using electron microscopy. These two parameters represent the volume of spines; hence, they can be used to deduce changes in spine size (Meng et al., 2002). Gross ultrastructural features of asymmetric glutamatergic synapses, synaptic density, and global distribution of spine head area or PSD length in *Sipa1l1*$^{-/-}$ mice, were all comparable to those of WT mice (Fig. 6*A*–*D*). These results suggested that SIPA1L1 is dispensable in spine growth and maturation, at least in hippocampal neurons.

We also performed electrophysiological experiments to address SIPA1L1 deficiency in synaptic transmission and NMDA-R-dependent plasticity. Paired-pulse facilitation (PPF) and input–output relationships of EPSPs in the hippocampal CA1 stratum radiatum showed no differences between *Sipa1l1*$^{-/-}$ and WT mice (Fig. 7*A*,*B*). This is consistent with the postsynaptic localization of SIPA1L1 and the similar spine size/density that exists between the genotypes. This result also suggests that no general depression of the AMPA-R mediated response occurred in *Sipa1l1*$^{-/-}$ hippocampus, which could have been resulted if Rap signaling was constitutively activated (Zhu et al., 2002, 2005). NMDA-R-dependent LTP induced by high-frequency stimulation was also comparable between the genotypes (Fig. 7*C*). Thus, SIPA1L1 may also be dispensable in actin reorganization and dynamic changes of spine morphology that underlie synaptic plasticity (Hotulainen and Hoogenraad, 2010).

We next considered the possibility of compensation by SIPA1L1 homologs. SIPA1L1 has two paralogs, denominated SIPA1L2 and SIPA1L3. Both proteins are localized to the postsynaptic compartment and interact with the LZTS family of proteins, similar to SIPA1L1 (Spilker et al., 2008; Dolnik et al., 2016). SIPA1L2 is also localized to presynaptic boutons and controls trafficking and signaling of TrkB-amphisomes (Andres-Alonso et al., 2019). However, SIPA1L2 does not colocalize with

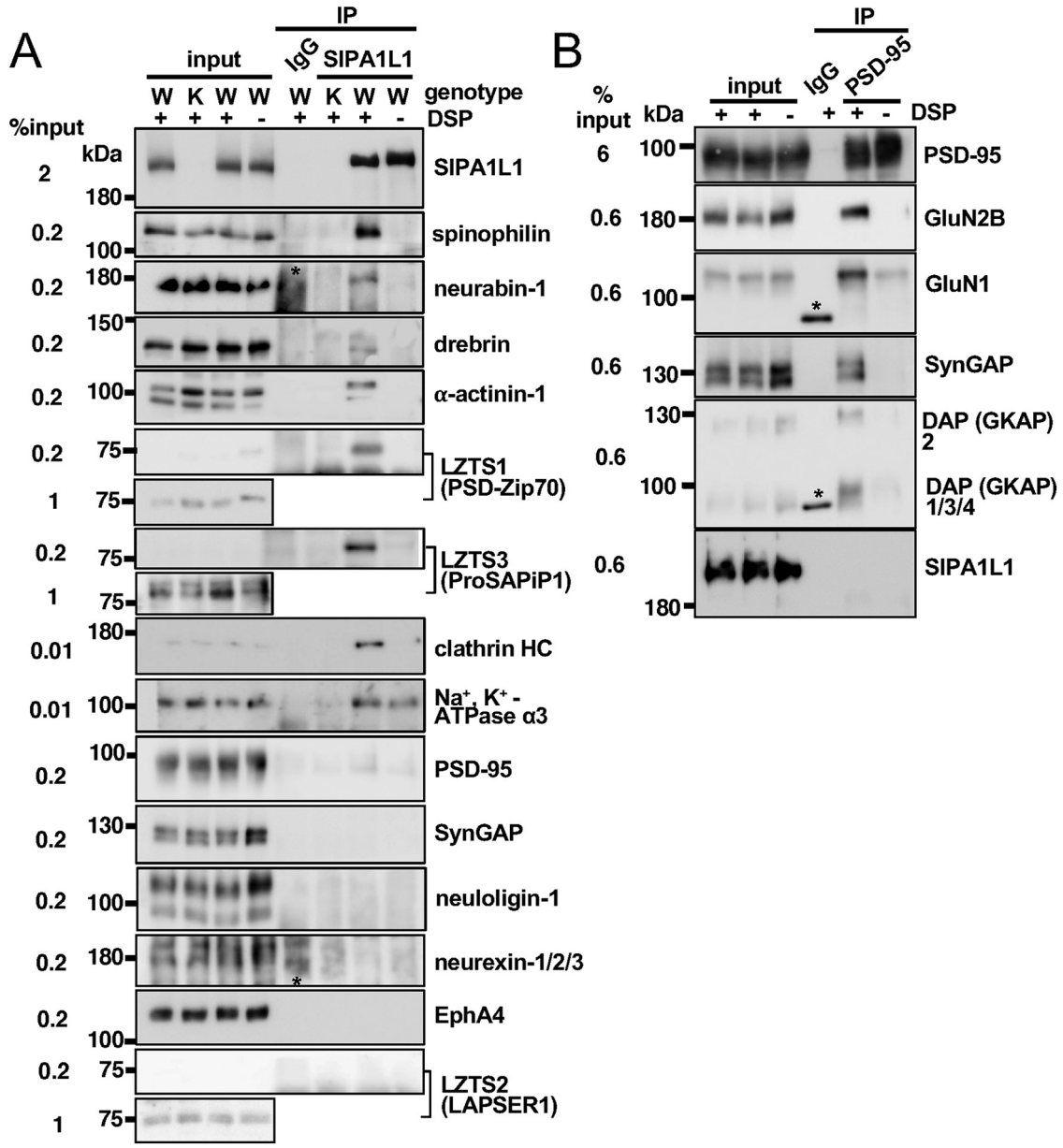

Figure 10. Confirmation of native interactors of SIPA1L1 using cIP-WB. ***A***, Confirmation of cIP-MS results by cIP-WB. The proportion of clathrin HC or Na^+, K^+-ATPase $\alpha 3$ co-precipitated with SIPA1L1 relative to the whole population was much smaller compared with other interactors. Detection of inputs for the LZTS family of proteins was performed separately with an increased amount, as they were not detectable with 0.2% input. Detection of a protein band in a control noncrosslinked lane, such as is seen in Na^+, K^+-ATPase $\alpha 3$, may suggest artifactitious postsolubilization interaction. ***B***, The same experiment was performed as in ***A*** except that anti-PSD-95 antibody was used for IP. *, nonspecific band.

F-actin when expressed in COS-7 cells nor does it induce spine growth in primary cultured neurons (Spilker et al., 2008). We found that expression of SIPA1L2 and SIPA1L3 was relatively higher in the hippocampus compared with other regions in WT brain, which was especially prominent for SIPA1L3 (Fig. 8*A–D*). However, we did not observe any significant change in expression level of SIPA1L2 or SIPA1L3 in *Sipa1l1*$^{-/-}$ hippocampus compared with WT (Fig. 8*E*,*F*). These results suggested little contribution of SIPA1L1 paralogs to compensate for SIPA1L1 deficiency.

Screening for native SIPA1L1 interactors in the brain identified spinophilin, neurabin-1, and drebrin

To find clues about the physiological function of SIPA1L1 and to clarify the discrepancy between the observed non-PSD localization of SIPA1L1 and reported SIPA1L1-interacting PSD-associated proteins, we performed screening for physiological SIPA1L1-interacting proteins. We adopted a chemical cIP strategy to preserve native interactions before addition of detergents. This strategy also enabled us to use stringent solubilization (2% SDS) and wash conditions to minimize nonspecific or artifactual interactions.

We performed cIP-MS screening in the mouse cerebral cortex and hippocampus, and identified 120 candidate SIPA1L1-interacting proteins (Fig. 9; Extended Data Fig. 9-1). We were able to successfully validate these interactions using cIP-WB on high-ranking proteins, which were mostly chosen based on mutual detection in both brain regions as general interactors (Fig. 10*A*). These included known SIPA1L1-binding proteins, such as a-actinin-1 (Hoe et al., 2009), LZTS1/PSD-Zip70 (Maruoka et al., 2005), LZTS3/Pro-SAPiP1 (Wendholt et al., 2006), as well as novel interactors, spinophilin/PP1R9B, neurabin-1/PP1R9A,

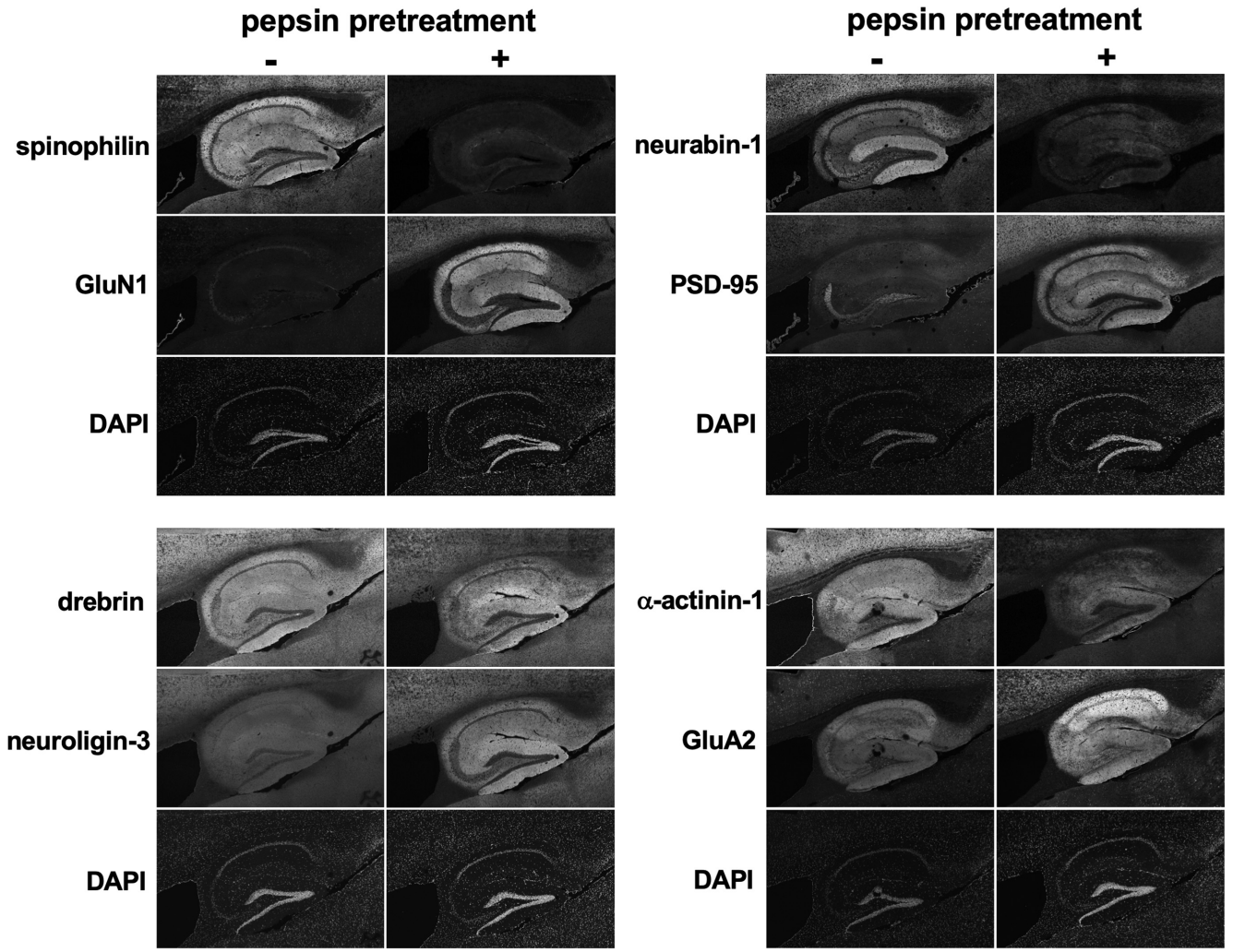

Figure 11. SIPA1L1-interacting proteins generally show non-PSD-like staining. Triple-stained confocal images of hippocampus on indicated proteins and DAPI on pepsin-pretreated (+) or pepsin-untreated (–) brain slices. Paired images are acquired and adjusted with identical settings and conditions. PSD proteins show strong staining with pepsin pretreatment, whereas SIPA1L1-interacting proteins show strong staining in untreated brain slices. Drebrin showed comparable level of staining in both conditions. Scale bar: 500 μm.

and drebrin. On the other hand, reported SIPA1L1 interactors (Pak et al., 2001; Nakayama et al., 2002; Roy et al., 2002; Meyer et al., 2004; Richter et al., 2007; Schmeisser et al., 2009) , including those that are strongly associated with PSD, namely, PSD-95, SynGAP, and neuroligin-1, failed to be reliably detected in cIP-WB (Fig. 10*A*). A parallel experiment on cIP-WB using an anti-PSD-95 antibody for IP resulted in successful detection of well-established PSD-95 interactors, such as GluN1, GluN2B, SynGAP, and DAP/GKAP, but not SIPA1L1 (Fig. 10*B*). Furthermore, the pepsin pretreatment-immunostaining analysis showed that SIPA1L1-interacting proteins tend to have stronger staining in pepsin-untreated brain slices, similar to SIPA1L1 (Fig. 11). This is consistent with reports showing their cytoplasmic localization in dendritic spines, although some of these proteins also localize to PSD (Muly et al., 2004a, b; Harris and Weinberg, 2012).

We attained additional confirmation by super-resolution colocalization analysis using the confined displacement algorithm (Figs. 12-14; Ramírez et al., 2010). Analyses in the neuropil of mouse hippocampus and cerebral cortex revealed highest colocalization of SIPA1L1 with spinophilin among the examined candidates (Fig. 15; Extended Data Fig. 15-1). Relatively high correlation of spinophilin and SIPA1L1 signals suggests a constant stoichiometric ratio in a complex. Analysis of somata and proximal neurites of CA1 pyramidal neurons showed that spinophilin aligns with SIPA1L1 along submembranous regions with occasional co-localization (Fig. 16; compare to Fig. 2*G*). Neurabin-1 and drebrin also showed significant colocalization and correlation with SIPA1L1 in the cerebral cortex (Fig. 15; Extended Data Fig. 15-1). However, colocalization of SIPA1L1 with neurabin-1 in hippocampus was much lower (Manders coefficient M2 = 0.062) compared with cerebral cortex (M2 = 0.179) and not significantly correlated (Extended Data Fig. 15-1). This may explain why neurabin-1 was detected in cerebral cortex by cIP-MS, but not in hippocampus (Extended Data Fig. 9-1). α-Actinin-1 also showed significant colocalization with SIPA1L1, albeit overlaps were quite small and without correlation. Clathrin heavy chain, Na^+, K^+-ATPase α3, or synaptophysin did not show significant colocalization or correlation with SIPA1L1 (Fig. 15; Extended Data Fig. 15-1).

We further confirmed that exogenous expression of SIPA1L1 and spinophilin in COS-7 cells successfully reproduced the SIPA1L1-spinophilin interaction without using a

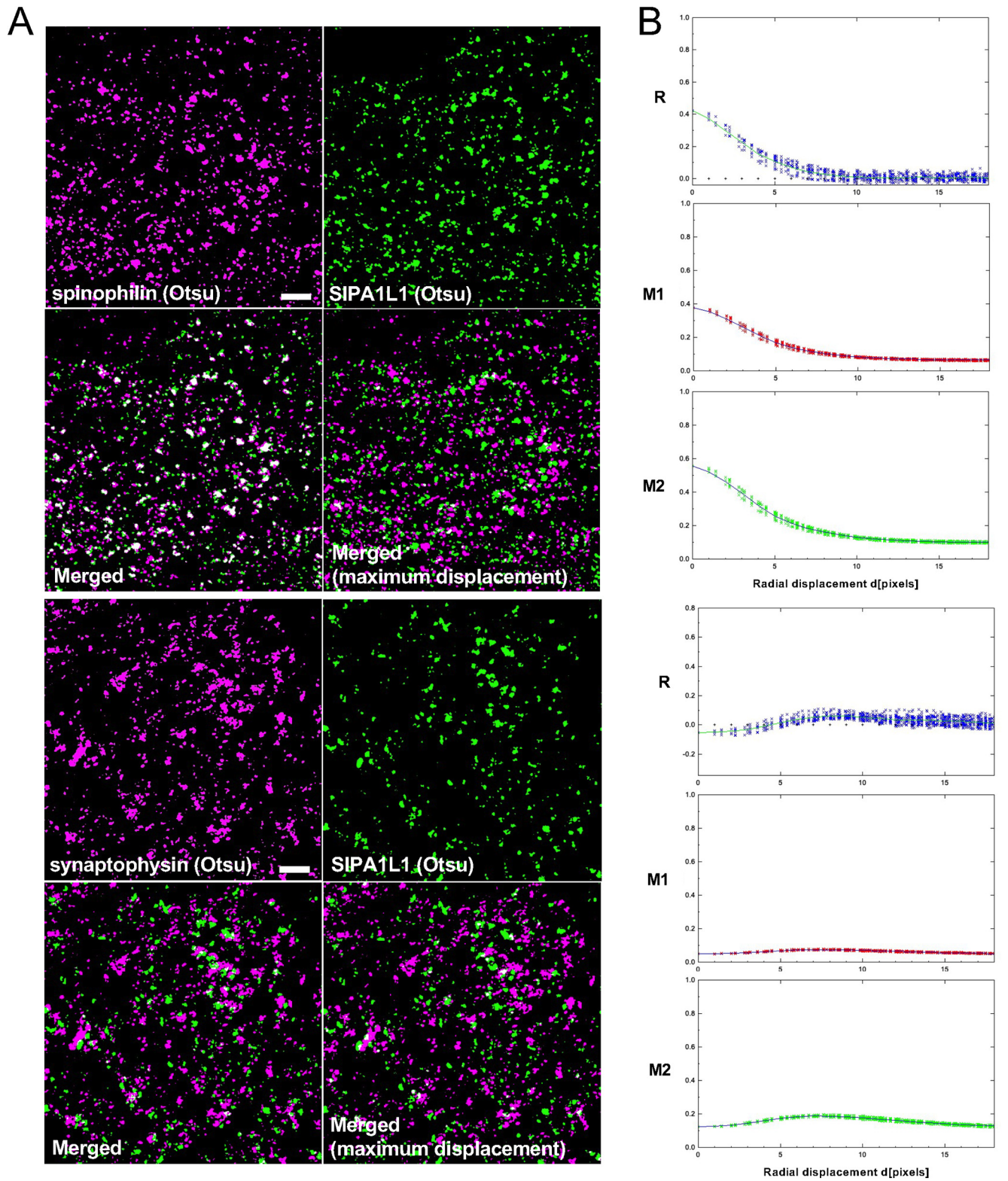

Figure 12. Co-localization analysis using the confined displacement algorithm. ***A***, Examples of super-resolution images converted by the Otsu method to define the background area. Otsu images were used to calculate the Manders coefficient, whereas raw images were used to calculate Pearson correlation coefficients. Random displacement images to calculate statistical significance were generated by translations in all directions at set distances (see Materials and Methods). Colocalization was analyzed on total 6724 mm^2 of neuropil area per protein pair. Scale bar: 2 μm. ***B***, *R*, Pearson correlation coefficient; M1, Manders coefficient for spiniophilin (top) or synaptophysin (bottom); M2, Manders coefficient for SIPA1L1.

crosslinker. The interaction depended on the C-terminal coiled-coil domain, but not on the N-terminal F-actin-binding domain of spinophilin. This result suggested that the SIPA1L1-spinophilin interaction is not mediated by F-actin (Fig. 17).

Taken together, our screening identified spinophilin as the most promising physiological interactor of SIPA1L1 in the brain, and also neurabin-1 and drebrin as strong candidates. LZTS1 and LZTS3 may also be *bona fide* interactors as they showed a

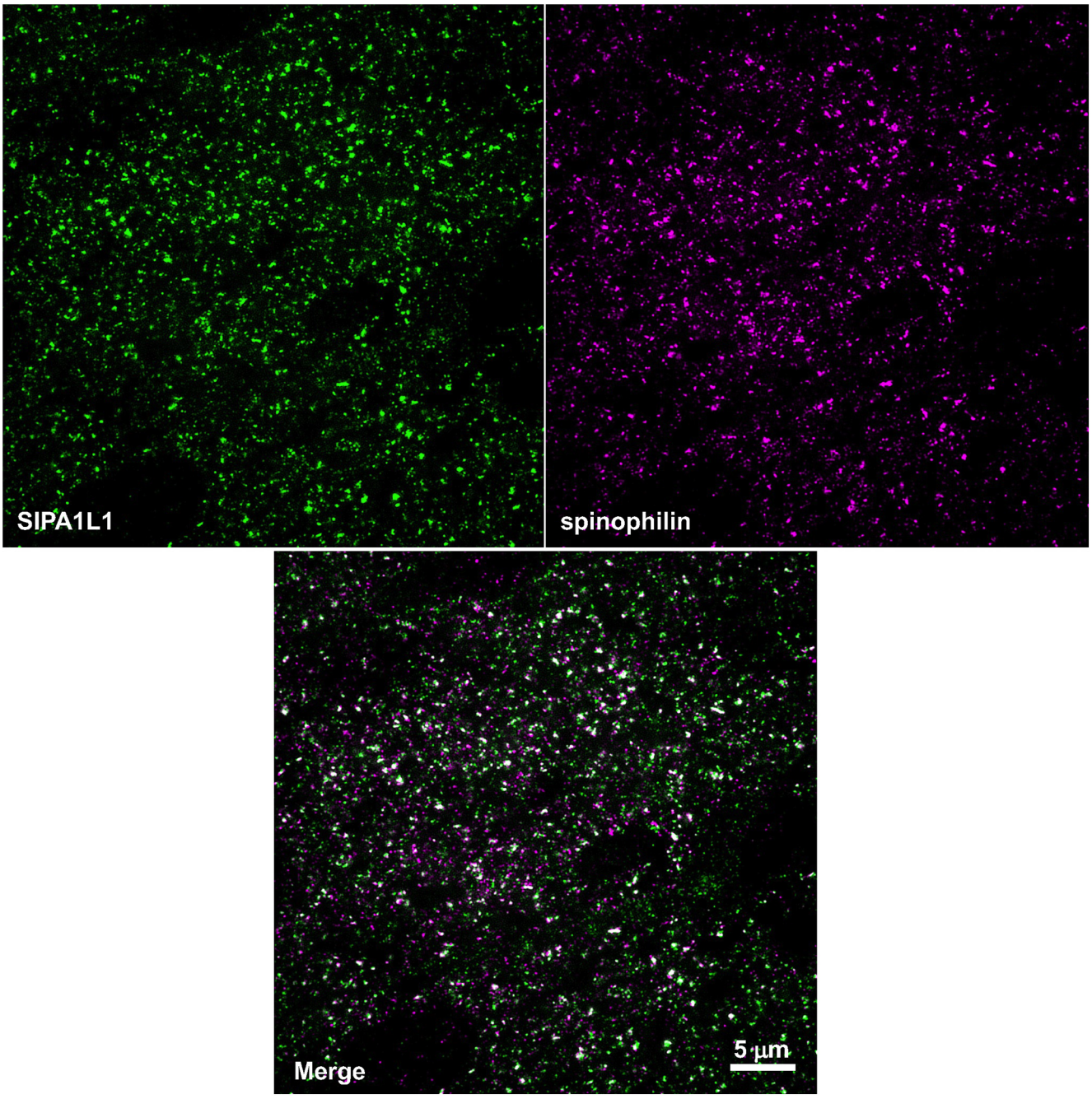

Figure 13. Original full super-resolution, double-staining images of SIPA1L1 and spinophilin. An example of a full original super-resolution image used in Figures 12, 15. For colocalization analysis, four raw serial Z-stack super-resolution images were used. Raw data are available at Mendeley https://doi.org/10.17632/f964whtpxh.1.

clear high proportion of co-IP with SIPA1L1 (Table 2 summarizes the results of the entire screening).

Sipa1l1$^{-/-}$ mice show aberrant responses to GPCR agonist stimulation and significantly enhanced epileptic seizure susceptibility

We next sought the functional relevance of the spinophilin-SIPA1L1 interaction. One of the most well-studied GPCR targets for spinophilin is α_2ARs. Spinophilin negatively regulates α_2-adrenergic responses by blocking the association of G protein receptor kinase 2 with agonist-receptor-G$\beta\gamma$ complexes, thereby antagonizing β-arrestin-2-dependent receptor endocytosis (Wang et al., 2004). As spinophilin-null (*Spn*$^{-/-}$) mice showed enhanced sensitivity to sedation elicited by α_2-adrenergic stimulation (Wang et al., 2004), we wondered how α_2-agonistic stimulation would affect the sedation response in *Sipa1l1*$^{-/-}$ mice. In the rotarod assay, *Sipa1l1*$^{-/-}$ mice were significantly more resistant to UK 14304-evoked sedation than WT mice (Fig. 18*A*), suggesting a possible inhibitory role of SIPA1L1-spinophilin interactions in spinophilin-mediated repression of the α_2-adrenergic response. To examine whether the resistance of *Sipa1l1*$^{-/-}$ mice to sedation is generalized or nonspecific in nature, we used another sedation-eliciting GPCR agonist, R-PIA, an agonist of adenosine A1 receptors. *Sipa1l1*$^{-/-}$ mice unexpectedly showed an enhanced response to R-PIA-stimulated sedation (Fig. 18*B*), similar to that of *neurabin-1*$^{-/-}$ mice (Chen et al., 2012). These results indicate a nongeneralized, GPCR-pathway-dependent sedation response in *Sipa1l1*$^{-/-}$ mice.

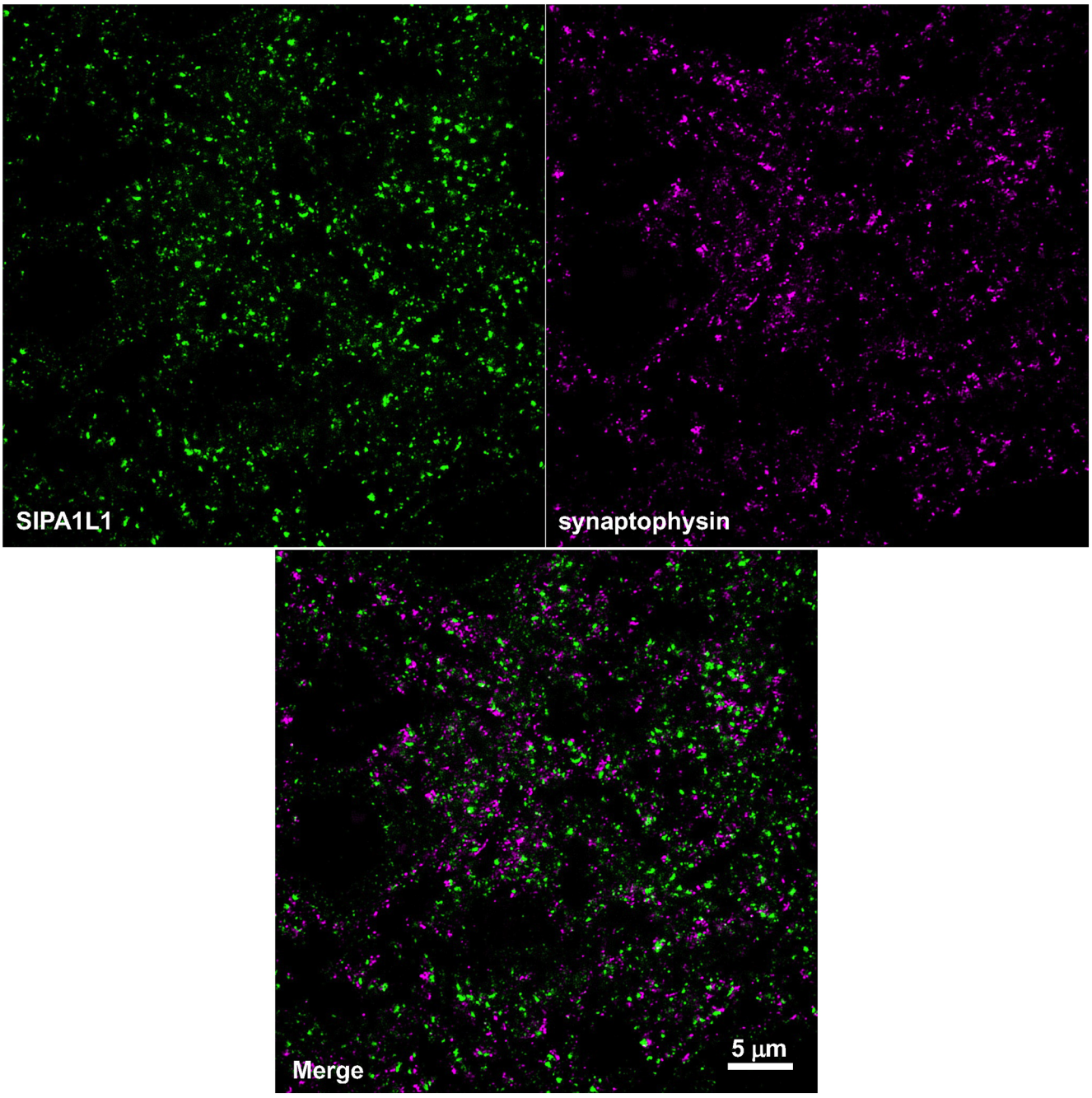

Figure 14. Original full super-resolution, double-staining images of SIPA1L1 and synaptophysin. An example of a full original super-resolution image used in Figure 12. For colocalization analysis, four raw serial Z-stack super-resolution images were used. Raw data are available at Mendeley https://doi.org/10.17632/f964whtpxh.1.

Another interesting phenotype observed in *Spn*$^{-/-}$ mice is their resistance to kainate-induced or PTZ-induced seizures (Feng et al., 2000). Although the mechanism underlying this phenotype is not well understood, several lines of evidence show that the neurotransmitter norepinephrine and α_2AR agonists exert powerful antiepileptogenic actions that are mediated by postsynaptic α_{2A}ARs, one of the three α_2AR subtypes (Szot et al., 2004). Moreover, α_{2A}AR mutant mice show significantly enhanced epileptic seizure susceptibility (Janumpalli et al., 1998). Thus, we hypothesized that *Sipa1l1*$^{-/-}$ mice might also have enhanced seizure susceptibility. Indeed, *Sipa1l1*$^{-/-}$ mice showed significantly enhanced susceptibility to kainate-induced or PTZ-induced seizures (Fig. 18*C*). An intraperitoneal injection of kainate (30 mg/kg) caused severe generalized tonic-clonic seizures (phase 4) in seven out of eight *Sipa1l1*$^{-/-}$ mice, whereas no WT mice (0/8) reached phase 4. A subconvulsive injected dose of PTZ elicited no generalized clonus (phase 3) in WT mice (0/8), but all *Sipa1l1*$^{-/-}$ mice (8/8) showed whole-body clonus with a sudden loss of upright posture.

We further asked whether α_{2A}-adrenergic stimulation could reverse the enhanced susceptibility of *Sipa1l1*$^{-/-}$ mice to PTZ-induced seizures. To this end, we administered the partial α_{2A}AR agonist, guanfacine (1 mg/kg), which has better therapeutic benefits than full agonists (Arnsten et al., 1988; Wang et al., 2007; Qu et al., 2019), 30 min before the PTZ injection. Guanfacine administration resulted in partial amelioration of seizure phenotypes in *Sipa1l1*$^{-/-}$ mice and three out of 8 mice did not show phase 3

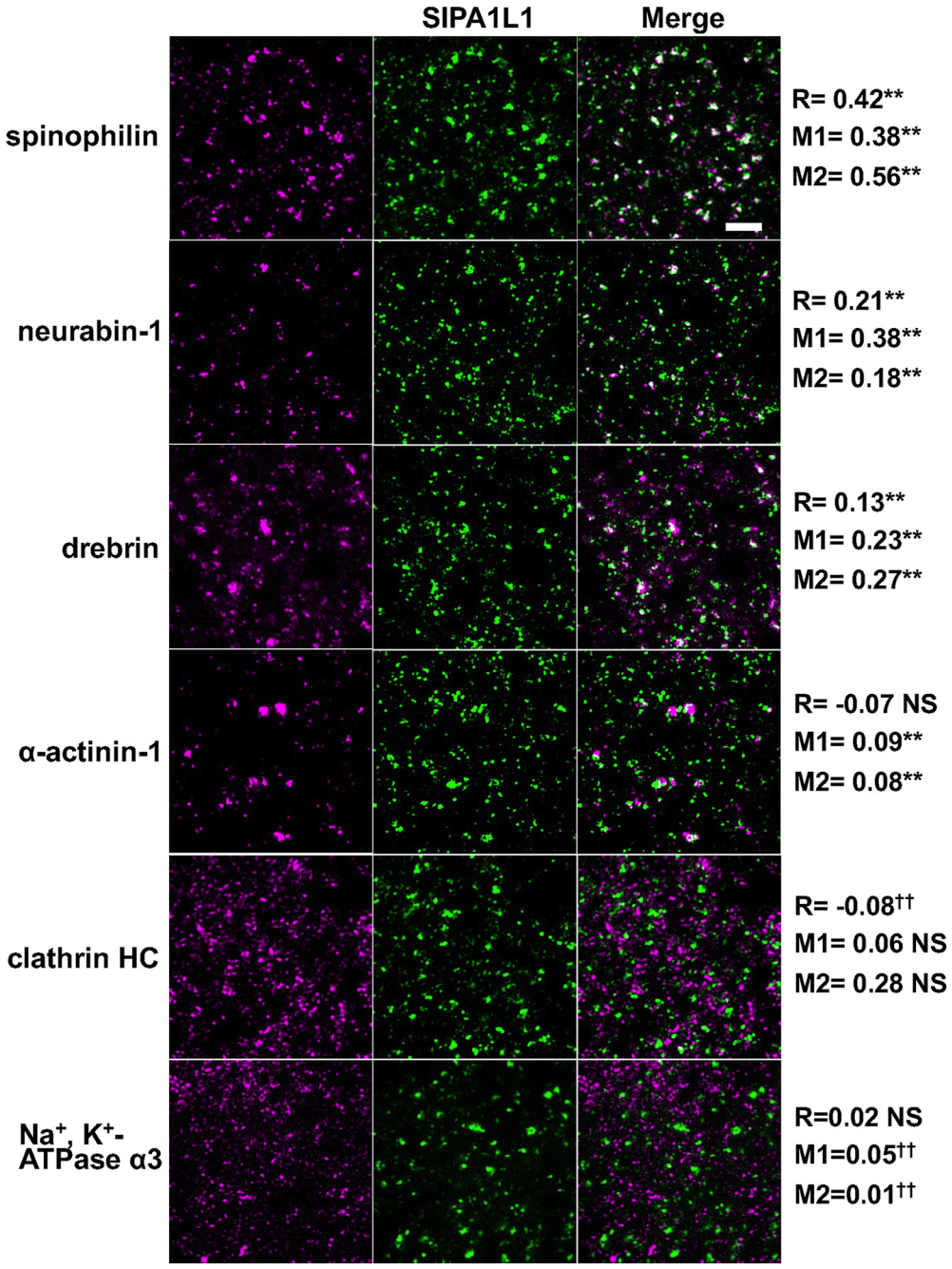

Figure 15. Spinophilin, neurabin-1, and drebrin show significant colocalization with SIPA1L1 in mouse cerebrum. Representative super-resolution immunofluorescence images of SIPA1L1 co-stained with indicated proteins in the neuropil of Layer V of the cerebral cortex. Colocalization was analyzed using the confined displacement algorithm on total 6724 mm^2 of neuropil area per protein pair. See Extended Data Figure 15-1 for more details and extended results. Raw image data are available at Mendeley https://doi.org/10.17632/f964whtpxh.1. *R*, Pearson correlation coefficient; M1 and M2, Manders coefficient for candidate interacting protein and SIPA1L1, respectively. $**p < 0.01$ (significant correlation or colocalization); †† $p < 0.01$ (significant noncorrelation or noncolocalization compared with random displacement images); NS, not significant. Scale bar: 2 μm.

seizures (Fig. 18*D*). This result suggested that enhanced susceptibility to PTZ-induced seizures is not developmentally fixed, but reversible and treatable by restoring α_{2A}-adrenergic activity, at least to some extent. However, the partial effect of guanfacine suggests that some other factors, e.g., other downstream targets of spiniophilin such as mGluRs, may also be involved (see Discussion).

Sipa1l1$^{-/-}$ mice show various types of behavioral impairment relevant to neuropsychiatric disorders

Since spinophilin is suggested to target various GPCRs, such as αARs, mAchRs, dopamine D2 receptors, μ-opioid receptors, and mGluRs, all of which are known to cause aberrant behaviors and to lead to neuropsychiatric disorders when dysregulated (for details, see Discussion), we investigated consequences of the loss of SIPA1L1 through a series of behavioral tests.

Sipa1l1$^{-/-}$ mice were born at the expected Mendelian ratio, were apparently healthy, and had lifespans similar to those of their WT littermates (773 ± 33 and 784 ± 36 d for WT and *Sipa111*$^{-/-}$, respectively; mean ± SEM; $N = 31$ and 38 for WT and *Sipa1l1*$^{-/-}$, respectively; $U = 532.5$, $p = 0.50$; two-tailed Mann–Whitney test). Gross anatomy of major organs, including brains of *Sipa1l1*$^{-/-}$ mice, was comparable to that of WT

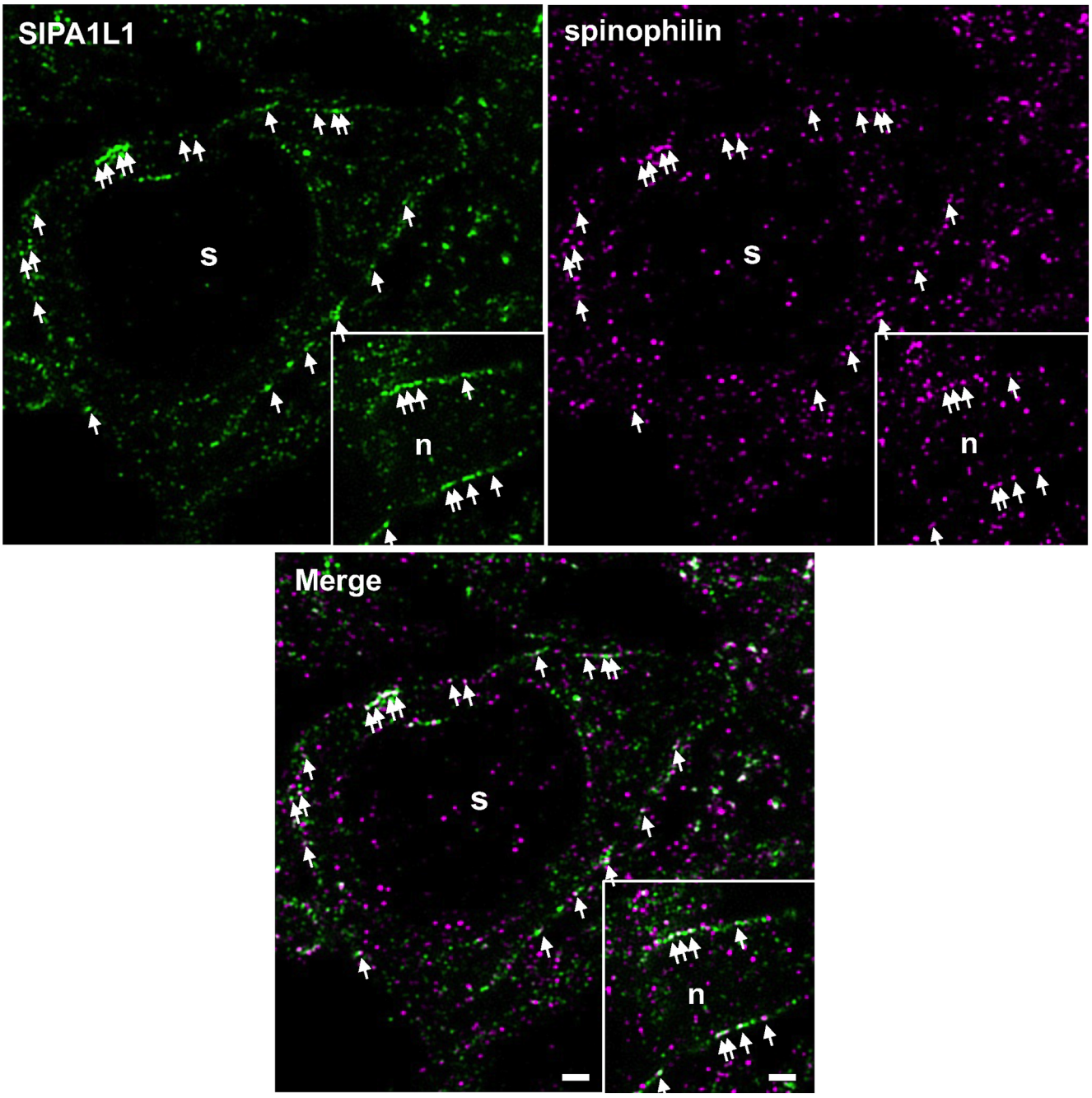

Figure 16. Spinophilin co-localizes with SIPA1L1 at the submembranous region in somata of neurons. Representative super-resolution immunofluorescence images of SIPA1L1 co-stained with spinophilin in the soma and proximal neurite (inset) of a pyramidal neuron in the hippocampal CA1 area. Arrows indicate examples of spinophilin aligned and colocalized with SIPA1L1 in the submembranous region (compare with Fig. 2*G*). s, soma; n, proximal neurite. Scale bar: 1 μm.

littermates, and distribution and expression levels of major synaptic proteins were not affected in the *Sipa1l1*$^{-/-}$ brain (Fig. 19). Nevertheless, *Sipa1l1*$^{-/-}$ mice showed striking hyperactivity in the open field test (Fig. 20*A*,*B*), with significantly less time spent in the center area and more time spent close to the walls, which is considered an indication of increased anxiety (Fig. 20*C*,*D*). In the light-dark transition test, despite increased locomotor activity, *Sipa1l1*$^{-/-}$ mice showed similar or slightly smaller transition numbers and significantly less time spent in the light chamber (Fig. 20*E*,*F*), also considered an indication of enhanced anxiety.

As SIPA1L1 expression is enriched in the cerebrum, which is highly involved in cognitive function such as learning and memory, we tested spatial learning by Morris water maze. Although *Sipa1l1*$^{-/-}$ mice showed slightly decreased performance compared with WT mice in the visible platform (nonspatial control) test (Fig. 20*G*), the difference was minimal and *Sipa1l1*$^{-/-}$ mice were able to achieve a level similar to WT mice by day 5 of the training (Extended Data Fig. 18-1). However, in the hidden platform test (Fig. 20*H*) and subsequent probe test (Fig. 20*I*), which requires coordinated action of various brain regions including the hippocampus and cerebral cortex (D'Hooge and De Deyn, 2001), *Sipa1l1*$^{-/-}$ mice showed severely impaired learning even after 10 d of training. In the test of classical eyeblink conditioning, an associative learning that is not influenced by activity level (Thompson and Kim, 1996; Takatsuki et al., 2003), *Sipa1l1*$^{-/-}$ mice showed normal learning in the delay paradigm (Fig. 20*J*),

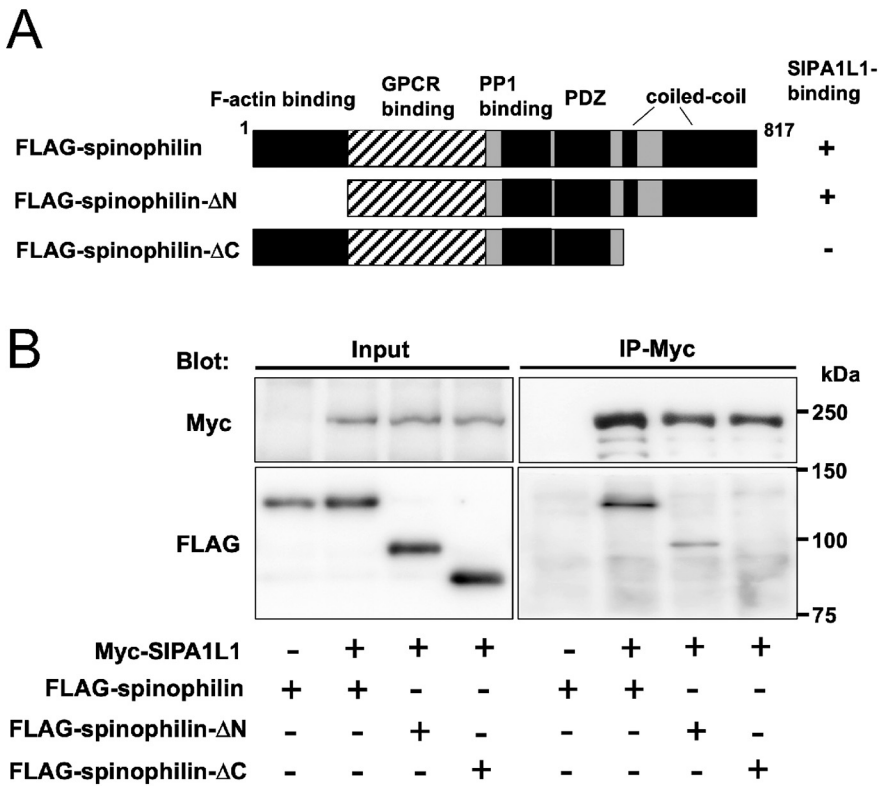

Figure 17. The SIPA1L1-spinophilin interaction in COS-7 cells. ***A***, Domain organization of spinophilin. A schematic structure of deletion mutants of spinophilin is shown. Positive binding activity is indicated as +. ***B***, Myc-tagged SIPA1L1 and indicated FLAG-tagged spinophilin constructs were exogenously co-expressed in COS-7 cells. The complex was immunoprecipitated with anti-Myc antibodies and interactions were examined by WB. Expressed constructs are indicated by +. The interaction depended on the C-terminal coiled-coil domain, but not on the N-terminal F-actin-binding domain of spinophilin.

Table 2. Summary of screening results for SIPA1L1-interacting proteins

UniProt accession	Gene symbol	Protein name	cIP-MS	cIP-WB	SR-coloc	Reference	Published method
Q6R891	*Ppp1r9b*	Neurabin-2, Spinophilin	CTX +++, HP +++	++	CTX ++, HP ++	Naovel	–
Q7TN74	*Ppp1r9a*	Neurabin 1	CTX +++, HP –	++	CTX ++, HP +	Novel	–
Q9QXS6	*Dbn1*	Drebrin	CTX +++, HP ++	++	CTX ++, HP+	Novel	–
P60853	*Lzts1*	Lzts1, PSD-Zip70	CTX ++, HP –	++	ND*	Maruoka et al. (2005)	Co-IP, ligand overlay binding
Q91YU6	*Lzts2*	Lzts2, LAPSER1	CTX –, HP –	–	ND*	Schmeisser et al. (2009)	Y2H, Co-IP
A2AHG0	*Lzts3*	Lzts3, ProSAPiP1	CTX +++, HP +++	++	ND*	Wendholt et al. (2006)	Y2H, Co-IP
Q7TPR4	*Actn1*	α-Actinin-1	CTX +++, HP +++	++	CTX +, HP +	Hoe et al. (2009)	Y2H, Co-IP
Q68FD5	*Cltc*	Clathrin heavy chain 1	CTX +++, HP ++	+	CTX –, HP –	Novel	–
Q6PIC6	*Atp1a3*	Na^+/K^+-ATPase α-3 subunit, Sodium pump subunit α-3	CTX +++, HP +++	+	CTX –, HP –	Novel	–
Q62108	*Dlg4*	Disks large homolog 4, PSD-95, SAP-90	CTX +, HP –	–	ND	Pak et al. (2001); Roy et al. (2002)	Y2H, Co-IP, GST pull-down
F6SEU4	*Syngap1*	Ras/Rap GTPase-activating protein SynGAP	CTX +++, HP –	–	ND	Pak et al. (2001)	Co-IP
Q9CS84	*Nrxn1*	Neurexin I-α	CTX –, HP –	–	ND	Nakayama et al. (2002)	Y2H
Q99K10	*Nlgn1*	Neuroligin-1	CTX –, HP –	–	ND	Meyer et al. (2004)	Y2H
Q03137	*Epha4*	Ephrin type-A receptor 4	CTX –, HP –	–	ND	Richter et al. (2007)	GST pull-down, Co-IP

CTX, cerebral cortex; HP, hippocampus; ND, not determined; co-IP, co-immunoprecipitation; Y2H: yeast two-hybrid screen; *, not performed because of a lack of suitable antibody. cIP-MS: +++, top 1/3 #PSMs; ++, middle 1/3 #PSMs; +, bottom 1/3 #PSMs; -, not detected or below cutoff line. cIP-WB: ++, ~0.1~% or more co-precipitated with 2–3% of SIPA1L1; +, ~0.01–0.1% co-precipitated with 2–3% of SIPA1L1; –, not reliably detected. Super-resolution colocalization analysis (SR-coloc): ++, significant colocalization and significant correlation; +, significant colocalization but nonsignificant correlation; –, nonsignificant colocalization and nonsignificant correlation.

which is dependent on cerebellum, brainstem, and thalamus network, but impaired learning in the trace paradigm (Fig. 20*K*), which is a more complex learning task that depends on several forebrain sites, including the hippocampus, prefrontal cortex and caudate nucleus in addition to the caudal brain regions noted above (Weiss and Disterhoft, 2011). Regarding cerebellar function, *Sipa1l1*$^{-/-}$ mice showed motor coordination and learning comparable to those of their WT littermates in the accelerating rotarod test (Fig. 20*L*), suggesting that cerebellar function is not much affected in *Sipa1l1*$^{-/-}$ mice.

In the three-chamber social interaction test, *Sipa1l1*$^{-/-}$ mice manifested significantly reduced interest in stranger mice (Fig. 20*M*,*N*), suggesting autistic-like behavior. Recently, it has been shown that the acoustic startle eyeblink response is enhanced in patients with autism spectrum disorder (ASD; Kohl et al., 2014; Takahashi et al., 2014). Enhanced acoustic startle response is also

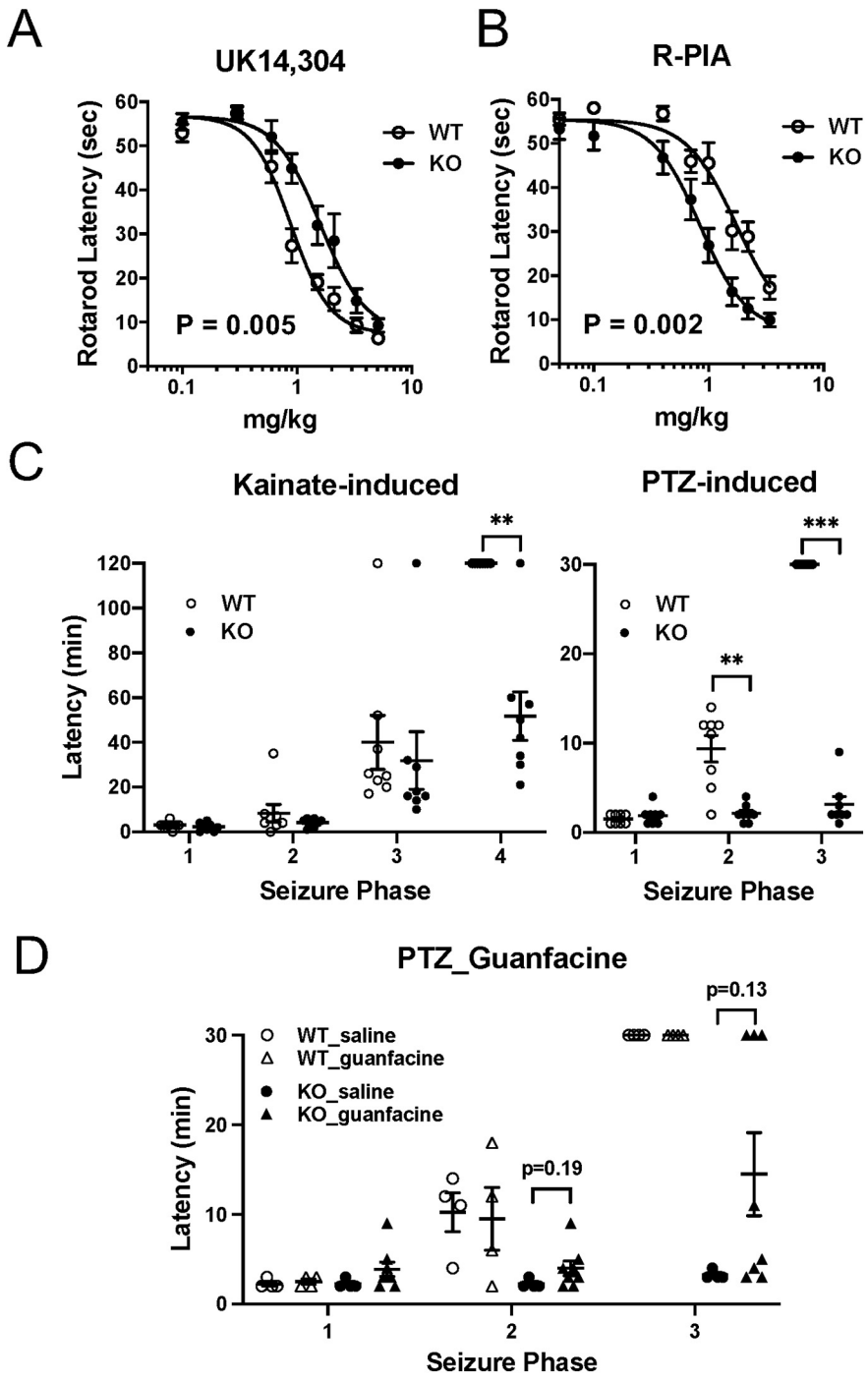

Figure 18. *Sipa1l1*$^{-/-}$ mice show aberrant responses to GPCR agonist stimulation and significantly enhanced epileptic seizure susceptibility. ***A***, ***B***, Sedation assessed by rotarod latency with increasing doses of α2AR agonist UK 14304 (***A***) or adenosine A1R agonist R-PIA (***B***). EC_{50} values for sedation in *Sipa1l1*$^{-/-}$ (KO) and WT mice are (***A***) 1.60 and 0.89 mg/kg, (***B***) 0.84 and 1.76 mg/kg, respectively. $N = 11–12$ per genotype. Values are mean ± SEM. *P* values indicate the genotype effect of two-way ANOVA. Partial η^2 for genotype effect are 0.19 (***A***) and 0.34 (***B***). ***C***, Latency to manifest kainate-induced or PTZ-induced seizures. ***D***, Reversal experiment with guanfacine on PTZ-induced seizures. Phase 1, hypoactivity; phase 2, partial clonus; phase 3, generalized clonus; phase 4, severe generalized tonic-clonic seizure (for details, see Materials and Methods). Cutoff times are 120 or 30 min for kainate-induced or PTZ-induced seizures, respectively. No WT mice manifested phase 4 or 3 for kainate-induced or PTZ-induced seizures, respectively. ***C***, $N = 8$ per genotype; ***D***, $N = 8$ for KO_guanfacine, $N = 4$ for others. Mean ± SEM is shown in the dot blots. Two-way ANOVA followed by Sidak's *post hoc* test. Partial η^2 for (***C***) genotype effect and (***D***) agonist effect for KO are (***C***) 0.30 (kinate) and 0.94 (PTZ) or (***D***) 0.20, respectively. $^{**}p < 0.01$, $^{***}p < 0.001$. Detailed statistical information is available in Extended Data Figure 18-1.

associated with fragile X syndrome (FXS), the most prevalent cause of intellectual disability that is frequently accompanied by hyperactivity, autism, and/or seizures (Koekkoek et al., 2005). We found that *Sipa1l1*$^{-/-}$ mice show an enhanced acoustic startle eyeblink response (Fig. 20*O*), similar to *Fmr1* mutant mice, a mouse model of FXS (Koekkoek et al., 2005).

Collectively, these results demonstrate critical roles of SIPA1L1 in multiple behaviors that are relevant to neuropsychiatric disorders, such as attention deficit hyperactivity disorder (ADHD), anxiety disorder, intellectual disability, ASD, or FXS.

Discussion

In this work, we have shown that, contrary to prevailing belief, SIPA1L1 is a not a major component of the PSD-95/NMDA-R complex, and is not even commonly localized to PSD. SIPA1L1 is suggested to be a cytoplasmic or submembranous protein distributed throughout neurons, interacting with the neurabin family of proteins, possibly to regulate GPCR signaling. *Sipa1l1*$^{-/-}$ mice showed striking behavioral anomalies without obvious changes in spine size distribution or NMDA-R-dependent synaptic plasticity, at least in the hippocampus. On the other hand, *Sipa1l1*$^{-/-}$ mice showed resistance or enhanced responses to α_2AR or adenosine A1 receptor agonist stimulation, respectively. However, our pharmacological and behavioral experiments are still preliminary in terms of SIPA1L1 involvement in spinophilin-mediated or neurabin 1-mediated GPCR regulation and require further in-depth investigations. Nevertheless, these results suggest that SIPA1L1 deficiency could result in serious behavioral abnormalities that may be relevant to neuropsychiatric disorders. This work could be an interesting starting point for new avenues of research on disorders that involve spinophilin-regulated or neurabin-1-regulated GPCR signaling.

The reasons for discrepancies between our work and previous studies are not all clear, but differences in materials and methods, e.g., primary cultured neurons versus neurons in mature brain or specificity of antibodies, may explain some of them. In addition, introduction of the cIP strategy, combined with stringent solubilization and wash conditions, certainly could have made a difference in co-IP experiments in terms of minimizing artifactual interactions. This is particularly true for proteins that could physically bind

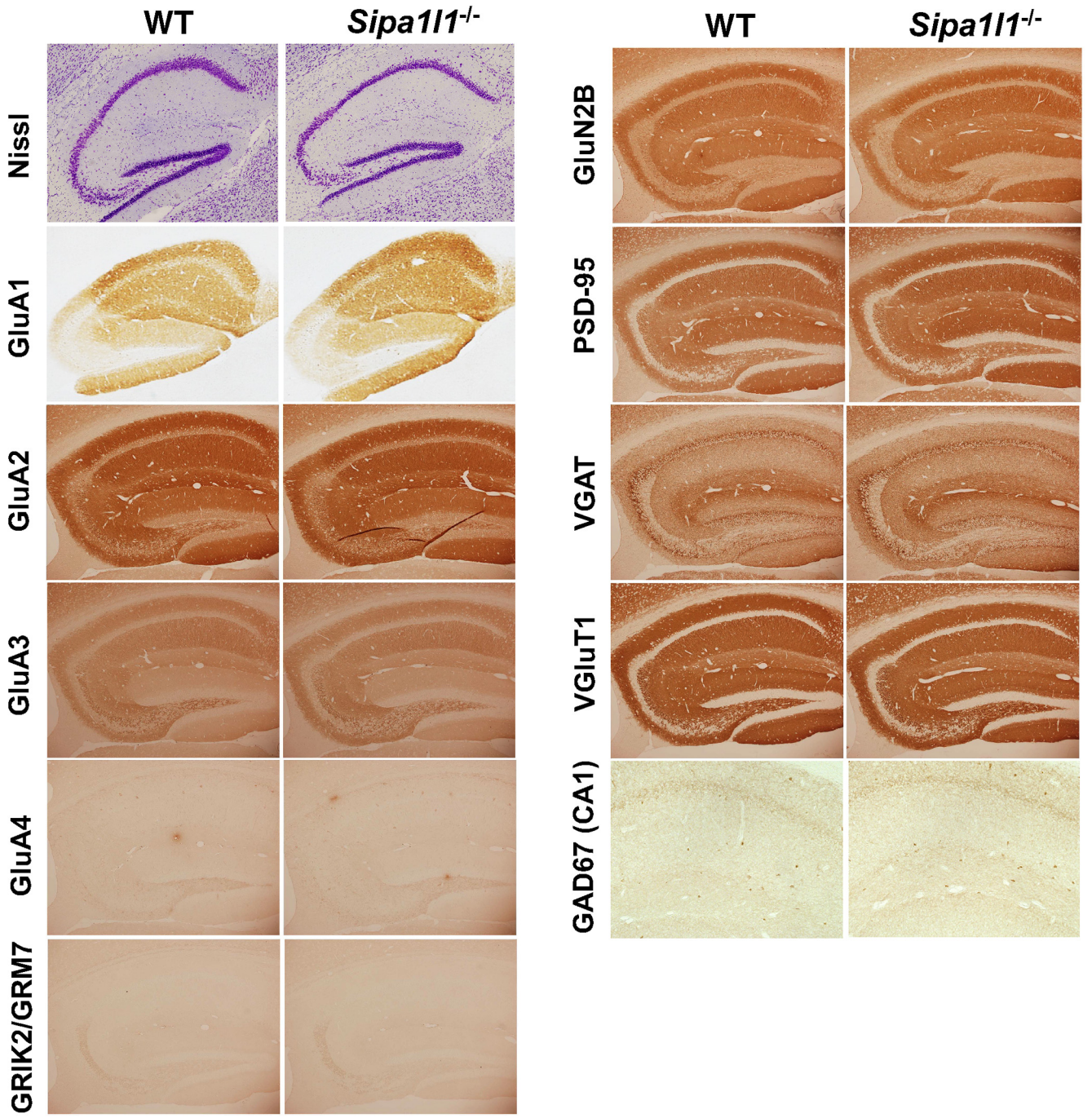

Figure 19. No gross defects in development of the *Sipa1l1*$^{-/-}$ brain. Representative data of Nissl staining, or immunostaining of synaptic marker proteins performed on adult *Sipa1l1*$^{-/-}$ mouse brains and those of WT littermates.

each other *in vitro*, such as the case for SIPA1L1 and PSD-95 (Roy et al., 2002). Proteins that require a strong detergent for solubilization and subsequent neutralization for antibody binding would have increased risk of artifactual interactions. We also speculate that since the actin cytoskeleton and its binding proteins are resistant to detergent solubilization (Hartwig and Shevlin, 1986; Cho et al., 1992; Allison et al., 2000), especially to nonionic detergent such as Triton X-100, non-PSD actin-binding proteins would be prone to contamination in conventional detergent extraction methods to determine PSD components. Thus, the pepsin pretreatment-immunostaining analysis could be a good alternative in determining the proportion of easy access (non-PSD) proteins and densely packed (PSD) proteins, as we have shown in this work. However, IEM will be the gold standard for conclusive results.

Frequent colocalization of SIPA1L1 and spinophilin throughout the cerebrum suggests that one of the major functions of SIPA1L1 involves interaction with spinophilin. This suggests an extrasynaptic and neuromodulatory role, involving some GPCRs that are targets of spinophilin. This hypothesis may explain some of behavioral anomalies in *Sipa1l1*$^{-/-}$ mice through aberrant modulation of neuronal firing properties and cognitive performance through extrasynaptic ion channels, without general change in spine size, synaptic density, or basic electrophysiological properties (Wang et al., 2007; Arnsten et al., 2012; Shine et al., 2021). In the case of α_2AR signaling, the simplest model may be

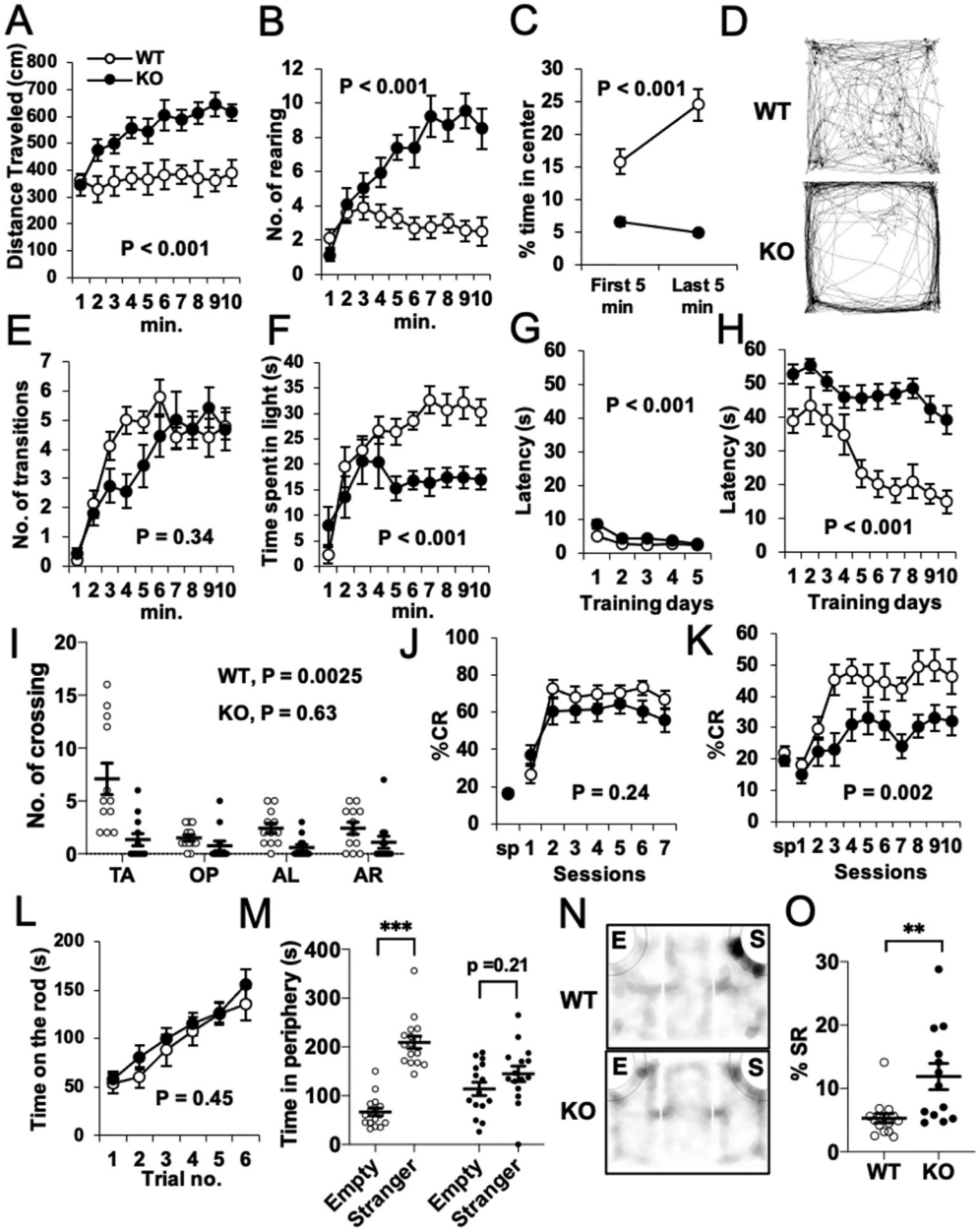

Figure 20. *Sipa1l1*$^{-/-}$ mice show various types of behavioral impairment relevant to neuropsychiatric disorders. ***A–D***, Open field test. ***D***, Representative traces of mice in a 50 × 50 cm arena during a 10-min test. A 30 × 30 cm area in the center of the arena is defined as the center in ***C***. ***E***, ***F***, Light-dark transition test. ***G–I***, Morris water maze. Control visible (***G***) and hidden (***H***) platform tests. Latency to reach the escape platform is shown. Mice were trained with six trials per day. In the probe test (***I***), the number of crossings of the original platform area or an equivalent area in each quadrant are shown. TA, target; OP, opposite; AL, adjacent left; AR, adjacent right. ***J***, ***K***, Eyeblink conditioning. Results from delay (***J***) and trace (***K***) paradigms are shown. CR, conditioned response; sp, spontaneous eye blinking. ***L***, Accelerated rotarod test. ***M***, ***N***, Three-chamber social interaction test. ***M***, Total time spent in the peripheral areas of an empty cage or a cage with a stranger mouse. ***N***, Representative heatmaps showing how long a mouse stayed in certain areas. E, empty cage; S, cage with stranger mouse. ***O***, The percentage of startle responses during the initial 30-ms period of the CS in eye blink conditioning. SR, startle response. Mean ± SEM is shown in line graphs and dot blots. $^{**}p < 0.01$, $^{***}p < 0.001$. *P* values labeled in line graphs indicate the genotype effect of two-way ANOVA. *P* values labeled in ***I*** indicate the quadrant effect of one-way ANOVA. $N = 12–18$. Detailed statistical information is available in Extended Data Figure 18-1.

that SIPA1L1-spinophilin interaction inhibits the spinophilin-α_2AR interaction, thus enhancing α_2AR signaling. αAR signaling participates in multiple brain functions, including cognition. α_2AR agonist stimulation could augment prefrontal cortex function, and guanfacine is currently used to treat ADHD (Tan and Limbird, 2006; Wang et al., 2007; Qu et al., 2019). One of the mechanisms underlying its efficacy may be targeting of hyperpolarization-activated cyclic nucleotide-gated (HCN) channels by α_{2A}AR signaling, which localizes to the extrasynaptic region of dendritic spines (Wang et al., 2007). Furthermore, $\alpha_{1B}AR^{-/-}$ mice showed hyperactivity and severely impaired learning in the Morris water maze (Spreng et al., 2001). Thus, downregulation of αAR signaling may contribute to some of the behavioral anomalies in *Sipa1l1*$^{-/-}$ mice.

Sipa1l1$^{-/-}$ mice showed many characteristics common to FXS, which include hyperactivity, anxiety, intellectual disability, altered sensorimotor integration, autistic behavior, and susceptibility to seizures. A possible link between SIPA1L1 and FXS may be regulation of Gp1 mGluRs via spinophilin (Di Sebastiano et al., 2016). In the compelling "mGluR theory," overactivation of mGluR function is postulated to mediate many symptoms of FXS, including learning deficits and seizure sensitivity (Lüscher and Huber, 2010). *Fmr1* mutant mice show enhanced mGluR-

LTD, whereas $Spn^{-/-}$ mice show decreased mGluR-LTD (Di Sebastiano et al., 2016). Interestingly, *Sipa1l1* mRNA binds FMR1 (an RNA-binding protein that regulates translation; Darnell et al., 2011) and SIPA1L1 translation is upregulated in juvenile, but significantly downregulated in adult *Fmr1* mutant mice (Tang et al., 2015; Ceolin et al., 2017). Although most protein expression was unchanged in adult *Fmr1* mutant brain, expression of 14 proteins, including SIPA1L1, was significantly downregulated to less than half, compared with WT control (Tang et al., 2015). As treatment by mGluR antagonists could ameliorate phenotypes of adult *Fmr1* mutant mice (Yan et al., 2005; de Vrij et al., 2008), downregulation of SIPA1L1 may contribute to overactivation of mGluR function in mature *Fmr1* mutant mice and possibly in FXS patients, by enhancing spinophilin function. Alternatively, downregulation of SIPA1L1 may simply contribute to behavioral anomalies of FXS in adulthood through other pathways. Whether SIPA1L1 has a role in regulating mGluRs and/or in FXS requires further study.

Dysregulation of other target GPCRs of spinophilin (μ-opioid receptors, mAchRs, and dopamine D2 receptors) or neurabin-1 (adenosine A1 receptors) may also contribute to some of the behavioral phenotypes in $Sipa1l1^{-/-}$ mice. μ-Opioid receptors are implicated in major depressive disorder (Peciña et al., 2019), whereas mAchRs are involved in schizophrenia and Alzheimer's disease (Foster and Conn, 2017). Dysregulation of the dopaminergic system has been implicated in a number of neuropsychiatric disorders and all currently available antipsychotics act via downregulation of dopamine D2 signaling (Foster and Conn, 2017). D2 signaling was recently implicated in ASD and may promote social avoidance (Pfaff and Barbas, 2019). Although regulation of dopamine D2 receptors by spinophilin is not well defined, $Spn^{-/-}$ mice may have downregulated D2 signaling (Allen et al., 2006). The SIPA1L1-neurabin-1 interaction could be related to the enhanced response of $Sipa1l1^{-/-}$ mice to stimulation with adenosine A1 receptor agonists.

To our knowledge, no genetic link between *SIPA1L1* and neuropsychiatric disorders has been identified to date, but it may be worth noting that putative causal DNA variation of *SIPA1L1* in exome sequencing data of Australian ASD cohort has recently been reported (An et al., 2014). Further detailed study of molecular mechanisms involving the SIPA1L1-spinophilin (or neurabin-1) interaction and their target GPCR pathways will enhance understanding of mechanisms of higher brain functions and may provide novel insight in studies of neuropsychiatric disorders.

References

Allen PB, Ouimet CC, Greengard P (1997) Spinophilin, a novel protein phosphatase 1 binding protein localized to dendritic spines. Proc Natl Acad Sci USA 94:9956–9961.

Allen PB, Zachariou V, Svenningsson P, Lepore AC, Centonze D, Costa C, Rossi S, Bender G, Chen G, Feng J, Snyder GL, Bernardi G, Nestler EJ, Yan Z, Calabresi P, Greengard P (2006) Distinct roles for spinophilin and neurabin in dopamine-mediated plasticity. Neuroscience 140:897–911.

Allison DW, Chervin AS, Gelfand VI, Craig AM (2000) Postsynaptic scaffolds of excitatory and inhibitory synapses in hippocampal neurons: maintenance of core components independent of actin filaments and microtubules. J Neurosci 20:4545–4554.

An JY, Cristino AS, Zhao Q, Edson J, Williams SM, Ravine D, Wray J, Marshall VM, Hunt A, Whitehouse AJ, Claudianos C (2014) Towards a molecular characterization of autism spectrum disorders: an exome sequencing and systems approach. Transl Psychiatry 4:e394.

Andres-Alonso M, Ammar MR, Butnaru I, Gomes GM, Acuña Sanhueza G, Raman R, Yuanxiang PAN, Borgmeyer M, Lopez-Rojas J, Raza SA, Brice N, Hausrat TJ, Macharadze T, Diaz-Gonzalez S, Carlton M, Failla AV, Stork O, Schweizer M, Gundelfinger ED, Kneussel M, et al. (2019) SIPA1L2 controls trafficking and local signaling of TrkB-containing amphisomes at presynaptic terminals. Nat Commun 10:5448.

Arnsten AF, Cai JX, Goldman-Rakic PS (1988) The alpha-2 adrenergic agonist guanfacine improves memory in aged monkeys without sedative or hypotensive side effects: evidence for alpha-2 receptor subtypes. J Neurosci 8:4287–4298.

Arnsten AF, Wang MJ, Paspalas CD (2012) Neuromodulation of thought: flexibilities and vulnerabilities in prefrontal cortical network synapses. Neuron 76:223–239.

Ceolin L, Bouquier N, Vitre-Boubaker J, Rialle S, Severac D, Valjent E, Perroy J, Puighermanal E (2017) Cell type-specific mRNA dysregulation in hippocampal CA1 pyramidal neurons of the fragile X syndrome mouse model. Front Mol Neurosci 10:340.

Charlton JJ, Allen PB, Psifogeorgou K, Chakravarty S, Gomes I, Neve RL, Devi LA, Greengard P, Nestler EJ, Zachariou V (2008) Multiple actions of spinophilin regulate mu opioid receptor function. Neuron 58:238–247.

Chen Y, Liu Y, Cottingham C, McMahon L, Jiao K, Greengard P, Wang Q (2012) Neurabin scaffolding of adenosine receptor and RGS4 regulates anti-seizure effect of endogenous adenosine. J Neurosci 32:2683–2695.

Cho KO, Hunt CA, Kennedy MB (1992) The rat brain postsynaptic density fraction contains a homolog of the Drosophila discs-large tumor suppressor protein. Neuron 9:929–942.

Darnell JC, Van Driesche SJ, Zhang C, Hung KY, Mele A, Fraser CE, Stone EF, Chen C, Fak JJ, Chi SW, Licatalosi DD, Richter JD, Darnell RB (2011) FMRP stalls ribosomal translocation on mRNAs linked to synaptic function and autism. Cell 146:247–261.

de Vrij FM, Levenga J, van der Linde HC, Koekkoek SK, De Zeeuw CI, Nelson DL, Oostra BA, Willemsen R (2008) Rescue of behavioral phenotype and neuronal protrusion morphology in Fmr1 KO mice. Neurobiol Dis 31:127–132.

D'Hooge R, De Deyn PP (2001) Applications of the Morris water maze in the study of learning and memory. Brain Res Brain Res Rev 36:60–90.

Di Sebastiano AR, Fahim S, Dunn HA, Walther C, Ribeiro FM, Cregan SP, Angers S, Schmid S, Ferguson SS (2016) Role of spinophilin in group I metabotropic glutamate receptor endocytosis, signaling, and synaptic plasticity. J Biol Chem 291:17602–17615.

Dolnik A, Kanwal N, Mackert S, Halbedl S, Proepper C, Bockmann J, Schoen M, Boeckers TM, Kühl SJ, Schmeisser MJ (2016) Sipa1l3/SPAR3 is targeted to postsynaptic specializations and interacts with the Fezzin ProSAPiP1/Lzts3. J Neurochem 136:28–35.

Feng J, Yan Z, Ferreira A, Tomizawa K, Liauw JA, Zhuo M, Allen PB, Ouimet CC, Greengard P (2000) Spinophilin regulates the formation and function of dendritic spines. Proc Natl Acad Sci USA 97:9287–9292.

Foster DJ, Conn PJ (2017) Allosteric modulation of GPCRs: new insights and potential utility for treatment of schizophrenia and other CNS disorders. Neuron 94:431–446.

Fujii S, Yamazoe G, Itoh M, Kubo Y, Saitoh O (2008) Spinophilin inhibits the binding of RGS8 to M1-mAChR but enhances the regulatory function of RGS8. Biochem Biophys Res Commun 377:200–204.

Fukaya M, Watanabe M (2000) Improved immunohistochemical detection of postsynaptically located PSD-95/SAP90 protein family by protease section pretreatment: a study in the adult mouse brain. J Comp Neurol 426:572–586.

Harris KM, Weinberg RJ (2012) Ultrastructure of synapses in the mammalian brain. Cold Spring Harb Perspect Biol 4:a005587.

Hartwig JH, Shevlin P (1986) The architecture of actin filaments and the ultrastructural location of actin-binding protein in the periphery of lung macrophages. J Cell Biol 103:1007–1020.

Hayashi S, Okada Y (2015) Ultrafast superresolution fluorescence imaging with spinning disk confocal microscope optics. Mol Biol Cell 26:1743–1751.

Hoe HS, Lee JY, Pak DT (2009) Combinatorial morphogenesis of dendritic spines and filopodia by SPAR and alpha-actinin2. Biochem Biophys Res Commun 384:55–60.

Hotulainen P, Hoogenraad CC (2010) Actin in dendritic spines: connecting dynamics to function. J Cell Biol 189:619–629.

Janumpalli S, Butler LS, MacMillan LB, Limbird LE, McNamara JO (1998) A point mutation (D79N) of the alpha2A adrenergic receptor abolishes the antiepileptogenic action of endogenous norepinephrine. J Neurosci 18:2004–2008.

Kobayashi S, Hida Y, Ishizaki H, Inoue E, Tanaka-Okamoto M, Yamasaki M, Miyazaki T, Fukaya M, Kitajima I, Takai Y, Watanabe M, Ohtsuka T, Manabe T (2016) The active zone protein CAST regulates synaptic vesicle

recycling and quantal size in the mouse hippocampus. Eur J Neurosci 44:2272–2284.
Koekkoek SKE, Yamaguchi K, Milojkovic BA, Dortland BR, Ruigrok TJH, Maex R, De Graaf W, Smit AE, VanderWerf F, Bakker CE, Willemsen R, Ikeda T, Kakizawa S, Onodera K, Nelson DL, Mientjes E, Joosten M, De Schutter E, Oostra BA, Ito M, et al. (2005) Deletion of FMR1 in Purkinje cells enhances parallel fiber LTD, enlarges spines, and attenuates cerebellar eyelid conditioning in fragile X syndrome. Neuron 47:339–352.
Kohl S, Wolters C, Gruendler TO, Vogeley K, Klosterkötter J, Kuhn J (2014) Prepulse inhibition of the acoustic startle reflex in high functioning autism. PLoS One 9:e92372.
Lee KJ, Lee Y, Rozeboom A, Lee JY, Udagawa N, Hoe HS, Pak DT (2011) Requirement for Plk2 in orchestrated ras and rap signaling, homeostatic structural plasticity, and memory. Neuron 69:957–973.
Lüscher C, Huber KM (2010) Group 1 mGluR-dependent synaptic long-term depression: mechanisms and implications for circuitry and disease. Neuron 65:445–459.
Maruoka H, Konno D, Hori K, Sobue K (2005) Collaboration of PSD-Zip70 with its binding partner, SPAR, in dendritic spine maturity. J Neurosci 25:1421–1430.
Meng Y, Zhang Y, Tregoubov V, Janus C, Cruz L, Jackson M, Lu WY, MacDonald JF, Wang JY, Falls DL, Jia Z (2002) Abnormal spine morphology and enhanced LTP in LIMK-1 knockout mice. Neuron 35:121–133.
Meyer G, Varoqueaux F, Neeb A, Oschlies M, Brose N (2004) The complexity of PDZ domain-mediated interactions at glutamatergic synapses: a case study on neuroligin. Neuropharmacology 47:724–733.
Muly EC, Smith Y, Allen P, Greengard P (2004a) Subcellular distribution of spinophilin immunolabeling in primate prefrontal cortex: localization to and within dendritic spines. J Comp Neurol 469:185–197.
Muly EC, Allen P, Mazloom M, Aranbayeva Z, Greenfield AT, Greengard P (2004b) Subcellular distribution of neurabin immunolabeling in primate prefrontal cortex: comparison with spinophilin. Cereb Cortex 14:1398–1407.
Nakanishi H, Obaishi H, Satoh A, Wada M, Mandai K, Satoh K, Nishioka H, Matsuura Y, Mizoguchi A, Takai Y (1997) Neurabin: a novel neural tissue-specific actin filament-binding protein involved in neurite formation. J Cell Biol 139:951–961.
Nakayama M, Kikuno R, Ohara O (2002) Protein-protein interactions between large proteins: two-hybrid screening using a functionally classified library composed of long cDNAs. Genome Res 12:1773–1784.
Pak DT, Sheng M (2003) Targeted protein degradation and synapse remodeling by an inducible protein kinase. Science 302:1368–1373.
Pak DT, Yang S, Rudolph-Correia S, Kim E, Sheng M (2001) Regulation of dendritic spine morphology by SPAR, a PSD-95-associated RapGAP. Neuron 31:289–303.
Peciña M, Karp JF, Mathew S, Todtenkopf MS, Ehrich EW, Zubieta JK (2019) Endogenous opioid system dysregulation in depression: implications for new therapeutic approaches. Mol Psychiatry 24:576–587.
Pfaff D, Barbas H (2019) Mechanisms for the approach/avoidance decision applied to autism. Trends Neurosci 42:448–457.
Qu L, Zhou Q, Xu Y, Guo Y, Chen X, Yao D, Han GW, Liu ZJ, Stevens RC, Zhong G, Wu D, Zhao S (2019) Structural basis of the diversity of adrenergic receptors. Cell Rep 29:2929–2935.e4.
Ramírez O, García A, Rojas R, Couve A, Härtel S (2010) Confined displacement algorithm determines true and random colocalization in fluorescence microscopy. J Microsc 239:173–183.
Richter KN, Revelo NH, Seitz KJ, Helm MS, Sarkar D, Saleeb RS, D'Este E, Eberle J, Wagner E, Vogl C, Lazaro DF, Richter F, Coy-Vergara J, Coceano G, Boyden ES, Duncan RR, Hell SW, Lauterbach MA, Lehnart SE, Moser T, et al. (2018) Glyoxal as an alternative fixative to formaldehyde in immunostaining and super-resolution microscopy. EMBO J 37:139–159.
Richter M, Murai KK, Bourgin C, Pak DT, Pasquale EB (2007) The EphA4 receptor regulates neuronal morphology through SPAR-mediated inactivation of Rap GTPases. J Neurosci 27:14205–14215.
Roy BC, Kohu K, Matsuura K, Yanai H, Akiyama T (2002) SPAL, a Rap-specific GTPase activating protein, is present in the NMDA receptor-PSD-95 complex in the hippocampus. Genes Cells 7:607–617.
Sagara M, Kawasaki Y, Iemura SI, Natsume T, Takai Y, Akiyama T (2009) Asef2 and Neurabin2 cooperatively regulate actin cytoskeletal organization and are involved in HGF-induced cell migration. Oncogene 28:1357–1365.
Satoh A, Nakanishi H, Obaishi H, Wada M, Takahashi K, Satoh K, Hirao K, Nishioka H, Hata Y, Mizoguchi A, Takai Y (1998) Neurabin-II/spinophilin. An actin filament-binding protein with one pdz domain localized at cadherin-based cell-cell adhesion sites. J Biol Chem 273:3470–3475.
Schmeisser MJ, Grabrucker AM, Bockmann J, Boeckers TM (2009) Synaptic cross-talk between N-methyl-D-aspartate receptors and LAPSER1-beta-catenin at excitatory synapses. J Biol Chem 284:29146–29157.
Seeburg DP, Feliu-Mojer M, Gaiottino J, Pak DT, Sheng M (2008) Critical role of CDK5 and Polo-like kinase 2 in homeostatic synaptic plasticity during elevated activity. Neuron 58:571–583.
Shine JM, Müller EJ, Munn B, Cabral J, Moran RJ, Breakspear M (2021) Computational models link cellular mechanisms of neuromodulation to large-scale neural dynamics. Nat Neurosci 24:765–776.
Smith FD, Oxford GS, Milgram SL (1999) Association of the D2 dopamine receptor third cytoplasmic loop with spinophilin, a protein phosphatase-1-interacting protein. J Biol Chem 274:19894–19900.
Spilker C, Acuña Sanhueza A, Böckers GA, Kreutz TM, Gundelfinger ED (2008) SPAR2, a novel SPAR-related protein with GAP activity for Rap1 and Rap2. J Neurochem 104:187–201.
Spreng M, Cotecchia S, Schenk F (2001) A behavioral study of alpha-1b adrenergic receptor knockout mice: increased reaction to novelty and selectively reduced learning capacities. Neurobiol Learn Mem 75:214–229.
Szot P, Lester M, Laughlin ML, Palmiter RD, Liles LC, Weinshenker D (2004) The anticonvulsant and proconvulsant effects of alpha2-adrenoreceptor agonists are mediated by distinct populations of alpha2A-adrenoreceptors. Neuroscience 126:795–803.
Takahashi H, Nakahachi T, Komatsu S, Ogino K, Iida Y, Kamio Y (2014) Hyperreactivity to weak acoustic stimuli and prolonged acoustic startle latency in children with autism spectrum disorders. Mol Autism 5:23.
Takatsuki K, Kawahara S, Kotani S, Fukunaga S, Mori H, Mishina M, Kirino Y (2003) The hippocampus plays an important role in eyeblink conditioning with a short trace interval in glutamate receptor subunit delta 2 mutant mice. J Neurosci 23:17–22.
Tan CM, Limbird LE (2006) The α2-adrenergic receptors: lessons from knockouts. In: The adrenergic receptors: in the 21st century. Totowa: Humana Press Inc.
Tang B, Wang T, Wan H, Han L, Qin X, Zhang Y, Wang J, Yu C, Berton F, Francesconi W, Yates JR 3rd, Vanderklish PW, Liao L (2015) Fmr1 deficiency promotes age-dependent alterations in the cortical synaptic proteome. Proc Natl Acad Sci USA 112:E4697–4706.
Thompson RF, Kim JJ (1996) Memory systems in the brain and localization of a memory. Proc Natl Acad Sci USA 93:13438–13444.
Valtschanoff JG, Weinberg RJ (2001) Laminar organization of the NMDA receptor complex within the postsynaptic density. J Neurosci 21:1211–1217.
Wang M, Ramos BP, Paspalas CD, Shu Y, Simen A, Duque A, Vijayraghavan S, Brennan A, Dudley A, Nou E, Mazer JA, McCormick DA, Arnsten AF (2007) Alpha2A-adrenoceptors strengthen working memory networks by inhibiting cAMP-HCN channel signaling in prefrontal cortex. Cell 129:397–410.
Wang Q, Zhao J, Brady AE, Feng J, Allen PB, Lefkowitz RJ, Greengard P, Limbird LE (2004) Spinophilin blocks arrestin actions in vitro and in vivo at G protein-coupled receptors. Science 304:1940–1944.
Weiss C, Disterhoft JF (2011) Exploring prefrontal cortical memory mechanisms with eyeblink conditioning. Behav Neurosci 125:318–326.
Wendholt D, Spilker C, Schmitt A, Dolnik A, Smalla KH, Proepper C, Bockmann J, Sobue K, Gundelfinger ED, Kreutz MR, Boeckers TM (2006) ProSAP-interacting protein 1 (ProSAPiP1), a novel protein of the postsynaptic density that links the spine-associated Rap-Gap (SPAR) to the scaffolding protein ProSAP2/Shank3. J Biol Chem 281:13805–13816.
Yan QJ, Rammal M, Tranfaglia M, Bauchwitz RP (2005) Suppression of two major fragile X syndrome mouse model phenotypes by the mGluR5 antagonist MPEP. Neuropharmacology 49:1053–1066.
Zhu JJ, Qin Y, Zhao M, Van Aelst L, Malinow R (2002) Ras and Rap control AMPA receptor trafficking during synaptic plasticity. Cell 110:443–455.
Zhu Y, Pak D, Qin Y, McCormack SG, Kim MJ, Baumgart JP, Velamoor V, Auberson YP, Osten P, van Aelst L, Sheng M, Zhu JJ (2005) Rap2-JNK removes synaptic AMPA receptors during depotentiation. Neuron 46:905–916.